# Neutrons at W 7-X

J. Junker, A. Weller

Max-Planck-Institut für Plasmaphysik

IPP 2/341 October 1998

**Abstract:** The W 7-X deutrium plasma (18 MW NI, 4 keV, $1.5 \cdot 10^{20}$ $m^{-3}$) will produce $6 \cdot 10^{16}$ neutrons during a 10 s pulse. A detailed geometrical model of the W 7-X experiment has been set up for the neutron transport calculations by the MCNP4B code (Monte Carlo Neutron Particle). The fast neutron flux (2.5 MeV) inside the torus is 100 times higher than inside the hall. The almost homogeneous thermal neutron flux inside the hall is reduced 30 times by doping the concrete walls with 700 ppm of boron. For a pulse scenario of 500 pulses per year the annual dose equivalent rate outside of the hall is down to the legally allowed level of 0.3 mSv/year, mainly by photons, due to the shielding of a 1.8 m thick concrete wall. The skyshine by the flux penetrating the 1.2 m thick concrete roof leads to 0.01 mSv/year at the fence. The structure of the experiment gets activated by the neutrons which for the chosen pulse scenario leads to a total activity varying between $2.6 \cdot 10^{9}$ and $1.2 \cdot 10^{13}$ Bq. The dominant isotopes are the superconductor compound ($^{28}Al$, $^{66}Cu$, $^{94m}Nb$) on the short timescale (min's) and the steel components ($^{51}Cr$, $^{54}Mn$, $^{60}Co$) on the long timescale (months and years). For the austenitic steel a concentration of 50 ppm of Co has been assumed. After 10 years lifetime of the experiment it takes 4.8 years until the long living $^{60}Co$ ($T_{1/2}$ = 5.3 years) becomes the dominant radioactice isotope. Having waited for totally 10 years the specific activity has almost come down to $1 \cdot 10^{5}$ Bq/to at which level a freely use of the material can be allowed. The Ar of the air gets activated up to the annual averaged activity of $2.34 \cdot 10^{10}$ Bq which by the forced ventilation of the hall leads to the average of 110 Bq/$m^3$ exhausted to the outside. The tritium produced by the deuterium collisions leads to 260 Bq/$m^3$. These emissions of radioactivity to the environment are below the legally tolerated values, about 2 times for Ar and 10 times for T. The neutrons deposit 3.6 kJ to the modular fiels coils most of which goes into to the fiberglass epoxy surrounding the superconductor windings. The energy deposed to the auxiliary field coils is 10 times less. Compared to the energy deposed by the neutrons the photon absorption is negligible for all coils.

# Content

# Introduction

Neutrons produced by fusion collisions open a wide field of plasma diagnostics. Evaluating the ion temperature of a keV plasma has been introduced already in the early days of the adiabatically heated theta pinches. Present day experiments, because of the successful increase of the triple product nτT (ion density and temperature, energy confinement time) by orders of magnitude, produce a such enormous number of neutrons that safety precautions have to be provided to a large extent. First of all the prompt neutron emission together with the induced photon radiation has to be shielded by concrete walls to get the biological dose equivalent down to a tolerable value. Next the activation of the structure material has to be considered. The activated materials restrict the access to the experiment for some time after any experimental procedure and require to wait for a substantial cooling down time after the lifetime of the experiment. Also the exhaust and dispersion of radioactivity to the environment must not be neglegted.

For the fusion reactor, and of course already for the ITER design, these problems are at the focus of the concept development. By the necessity of using tritium in addition to deuterium as the working gas one cannot go around the problem of developing and installing the complicated equipment for a safe handling of tritium gas. But the high enrgetic neutron flux finally represents the energy source the reactor is aiming for.

Wendelstein 7-X (W 7-X), the Stellarator experiment presently under construction, has the scientific aim to demonstrate the improved confinement of the optimized magnetic field configuration for a high temperature plasma in the reactor relevant long mean free path regime. To reach this goal it is fully sufficient to operate with deuterium. There is no need for any tritium. Therefore no experimental equipment will be foreseen to handle tritium.

The basic fusion reactions in a deuterium plasma are the following:

- 2.5 MeV neutrons are released by the $D(d,n)^3He$ process governed by the rate coefficient for the temperature of the deuterons or the energy of the injected deuterium ions,
- tritons of 1 MeV result from the D(d,p)T process at the same rate as the 2.5 MeV neutrons,
- the tritons colliding with the deuterons produce 14 MeV neutrons by the D(t,n) reaction at a very low level compared to the 2.5 MeV rate.

Although the activation cross section for the high energetic neutrons is pretty high this „burn up“ process usually can be neglegted. All results within this report refer to the 2.5 MeV neutron flux only.

The results worked out in this report start by evaluating the neutron rate from the plasma parameters and the injection data taking into account a reasonable operation scenario. The neutron transport has been descibed by a Monte Carlo calculation for which a detailed geometry model of the W 7-X experiment has been set up. The neutron fluxes and their energetic distributions are desribed. Studies on the shielding by concrete walls have been done. The activation of the structure and the air with the resulting activities have been calculated. A study of the cooling down period after the shutdown of the experiment with the advantageous effect of a low cobalt concentration has been done. The radioactivty in the environment has been dicussed to some extent. Finally the energy deposed to the superconductor has been evaluated.

All the details necessary to operate the Monte Carlo code have been given in the appendix which contains the full input file for the MCNP code.

# Neutron source W 7-X

## Plasma Parameters

Wendelstein 7-X will be equipped with three heating systems: ECRH, ICRH, and NI. The well established ECRH at 140 GHz is planned to operate stationary at the power level of 10 MW. The other heating sytems will be set up in two stages. Stage I encompasses ICRH at 4 MW and NI at 4.5 MW. At stage II the power of NI will be increased up to 18 MW pulsed for 10 s.

The high performance plasma parameters - high density, high ion temperature, and high $\beta$ - are expected to be realized for the stage II NI heated plasma. This will allow to explore the predicted $\beta$ limit as well as the maximum achievable $nT\tau$ value which are the major scientific aims of the W 7-X experiment. With respect to the neutron production, we only consider in the following the high performance plasma parameters produced by 18 MW NI heating power.

The plasma ion temperature and its radial profile are calculated by solving the stationary one-dimensional heat transport equation by using the numerical code TEMPL. The ion density is taken equal to the electron density. The central density is assumed to be $1.5 \cdot 10^{20}$ m$^{-3}$. The density profile is kept constant in time and similar in shape to the measured profiles at the W 7-AS experiment (Fig. 1).

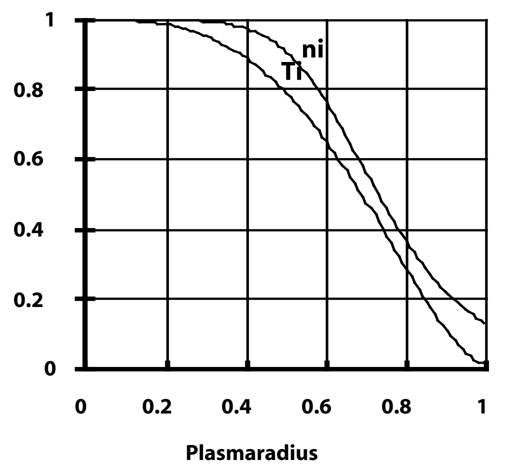


Figure 1. Radial profiles of $T_i$ (calculated from TEMPL) and $n_i$ (as measured at W 7-AS)

In the central region of the plasma, electrons and ions are heated by injecting 65 keV deuterons at the power level of 18 MW. Under the assumption that the theoretically predicted improvement of the energy confinement will be verified, the ion heat conduction will be reduced to $^1/_8$ of its neoclassical value. Taking this into account the TEMPL code delivers a central ion temperature of 4 keV which falls to 2 keV at about 0.6 of the plasma radius. The experimental parameters and the data of the plasma are listed in Table I.

Table I. Parameters of the experiment and of the NI heated Plasma

| | |
|---|---|
| Torus radius | $R = 5.5$ m |
| Plasma radius | $r = 0.53$ m |
| Magnetic field | $B_0 = 2.5$ T |
| Rotational transform | $\iota = 0.85$ |
| Heating power | $P_{NI} = 18$ MW |
| D particle energy | $E_D = 65$ keV |
| Ion density | $n_{i0} = 1.5 \cdot 10^{20}$ m$^{-3}$ |
| Ion temperature | $T_{i0} = 4.0$ keV |
| 50 twisted modular field coils (mf coils) | |
| 20 plane but tilted auxiliary field coils (af coils) | |

## Operation Scenario

Ultimately stellarators promise stationary reactor operation, and W 7-X is designed that this property can be demonstrated for the reactor relevant long-mean-free-path regime. The ECRH heating equipment will be capable of producing a stationary plasma. The high power NI at 18 MW, although pulsed for 10 s, will heat the plasma up to 4 keV and still reach stationary conditions for most of the pulse duration. For calculating the total neutron production, the peak parameters are taken into account for the full length of the NI pulse.

Experiments to achieve the high temperature, high density plasma will be done first with light hydrogen both for the plasma and for the injected particles until the high performance quality of the plasma can be demonstrated. This allows to run the experiment without any precautions with respect to the neutron production. Having progressed with the experiment to successfully demonstrate the high performance quality of the plasma one will turn to deuterium. One particular advantage using deuterium for the injected particles is to increase the heating power without any loss of efficiency for the neutralization. (Deuterons have twice the energy of protons at the same speed.) Also the isotope effect on the plasma confinement will be studied. Neutrons emitted from the plasma will be used for a variety of diagnostics. Flux measurements, energy distributions, temporal behaviour, and probe activations will be measured to determine e.g. the ion temperature and ist temporal and space resolved distribution.

The neutron induced activation of the structure will limit the access to the experiment. Therefore, the number of high performance pulses and their rate will be kept low whenever feasible. The following operation scenario for the high performance pulses appears reasonable and will be used as a reference for the assessment of the safety issues:

- 10 s per pulse,
- 1 **pulse** every 20 min.,
- 1 **series** of 10 pulses per day,
- 1 **period** of 5 days per week,
- 1 **campaign** of 5 weeks per ½ year,
- total **lifetime** of 10 years, i.e. 20 campaigns.

Summarizing, W 7-X operates with a plasma at high performance for totally

- **500 pulses** or **1.4 h per year**, and
- **5 000 pulses** or **13.9 h per 10 years lifetime**.

Fig. 2 shows a graphical presentation of this operating scenario. On a logarithmic time scale are plotted

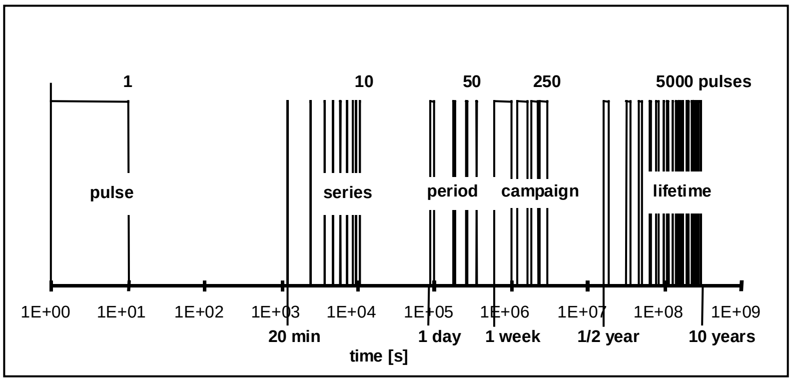

Figure 2. Operation scenario for high performance pulses

the lengths of a pulse, of a series, of a period, of a campaign, and of the lifetime of the experiment with 5 000 pulses alltogether.

## Neutron Production

Fusion collisions between deuterons lead to the process D(d,n)$^3$He which releases neutrons at 2.5 MeV. Another branch of fusion collisions with the same probability leads to D(d,p)T which releases tritons at 1 MeV. These tritons have a high probability to burn up by the process D(t,n)α which finally produces neutrons at 14 MeV, which is the essential energy delivering process for the fusion reactor. For W 7-X, this process of 14 MeV neutron production is of minor importance, however, because the triton density is very low compared to the deuterium density.

In a deuterium plasma heated by deuterium injection there are two classes of particles: the plasma particles described by their thermal distribution and the high energetic beam particles described by their slowing down distribution. Neutrons are produced by collisions between the following partners:

- **plasma** particles with **plasma** particles (p-p),
- **beam** particles with **plasma** particles (b-p), and
- **beam** particles with **beam** particles (b-b)

The rate coefficients[1,2] for the neutron production have been evaluated[3] taking the radial profiles of the temperature and of the density into account.

**Plasma** particles colliding with **plasma** particles produce neutrons according to a rate coefficient which has to be averaged over the velocity distribution of the thermal deuterons. At $T_{i,0}$ = 4 keV the rate coefficient is $<\sigma v> = 4.45 \cdot 10^{-26}\,m^3/s$. Integrating the temperature dependent rate over the whole plasma volume, taking into account the $T_i$ and $n_i$ profiles, delivers the neutron production rate

$$R_{p-p} = \int \frac{n_i^2}{2} < \sigma v > dV = 3.3 \cdot 10^{15} s^{-1}.$$

**Beam** particles colliding with **plasma** particles produce neutrons according to the rate coefficient given for the the monoenergetic fast beam particles and the relatively slow plasma particles which can be considered to be at rest. For the full deuteron energy $E_0$ = 65 keV the rate coefficient is $(\sigma v)_0 = 2.01 \cdot 10^{-24}\,m^3/s$. For the injected deuterium beam it is assumed that 85% of the beam particles are at full energy of 65 keV and 80% of the beam power of 18 MW get absorbed by the plasma. Together with the energy loss time[4] $\tau_0$ = 28.4 ms (by collisions with electrons and ions) for the full energy particles the stationary density of the fast particles is $n_b = 4.45 \cdot 10^{18}\,m^{-3}$. This results

[1] A.Peres, J. of Appl. Physics, **50**, 9, p 5569 (1979)
[2] H.S. Bosch, G.M. Hale, Nucl. Fus., **32**, 4, p. 611 (1992)
[3] J.Junker, The FORMEX Plasma Formulary, Lab. Report IPP 2/323 (1994)
[4] B.A.Trubnikov: Review of Plasma Physics (Ed. M.A.Leontovich), Consultant Bureau N.Y., **1**, p. 105 (1965)

from the simplifying and overestimating assumption that all the fast particles fill up the central region up to ½ of the plasma radius where the ion density is highest and almost constant. The energy distribution of the slowing down particles has been evaluated from: $dn_b(E) = \dot{n}_b \cdot dt / dE = n_b \cdot \tau / \tau_0 \cdot dE / E$. For the neutron production rate one gets

$$R_{b-p} = Vol \cdot n_b n_i (\sigma v)_0 \int_0^{E_0} \frac{\tau}{\tau_0} \frac{\sigma v}{(\sigma v)_0} \frac{dE}{E} = 2.7 \cdot 10^{15} s^{-1}.$$

There are almost equal contributions to the neutron production rate from the p-p collisons and the b-p collisions. Neglecting the correction by the slowing down integral, i.e. keeping the injected particles at full energy for all their lifetime, would lead to the overestimated rate of $1.0 \cdot 10^{16}$ $s^{-1}$ for the b-p collisions.

**Beam** particles colliding with **beam** particles have been considered in an even more simplified manner. For calculating the neutron rate all beam particles have been kept at full energy. The resulting rate coefficient is $(\sigma v)_0 = 1.17 \cdot 10^{-23}$ $m^3/s$ .Together with the beam particle density and the volume filled by the beam particles as discussed above one gets for the neutron production rate

$$R_{b-b} = \frac{n_b^2}{2} (\sigma v)_0 \cdot Vol = 8.7 \cdot 10^{14} s^{-1}.$$

Summing up all the neutron production rates for the 2.5 MeV neutrons results into the total neutron production rate

$$\boxed{R_{2.5MeV} = R_{p-p} + R_{b-p} + R_{b-b} = 6 \cdot 10^{15} s^{-1}.}$$

All the simplified assumptions for the individual neutron production rates lead to an overestimation. Therefore the summarized neutron production rate has been lowered by about 15% to get $6 \cdot 10^{15}$ $s^{-1}$ as a reference figure. This value for the instantaneous neutron production rate has been taken for all the following calculations. Together with the pulse scenario decribed before this instantaneous neutron production rate leads to the annual neutron rate of $3 \cdot 10^{19}$ $y^{-1}$ or the annual averaged neutron rate of $1 \cdot 10^{12}$ $s^{-1}$. The latter is the relevant figure for all the dose calculations. The radial distribution of the neutron production rate, weighted by the plasma radius, peaks at 40% of the plasma radius.

The deuteron collisions by the D(d,p)T reaction, produce also 1 MeV tritons at the same rate as the 2.5 MeV neutrons from the D(d,n)$^3$He reaction. These tritons colliding with the plasma deuterons lead to the burn up process producing 14 MeV neutrons by the D(t,n)α reaction. For W 7-X because of the very low density of the tritons the 14 MeV neutron production rate is negligible compared to the 2.5 MeV neutron production rate. The production rate for the 14 MeV neutrons is estimated by its upper limit assuming all tritons staying at the full enery of 1 MeV during their lifetime which is taken to be their slowing down time. One gets for the rate coefficient $(\sigma v)_0 = 3.3 \cdot 10^{-22}$ $m^3/s$, and from the production rate of $6 \cdot 10^{15}$ $s^{-1}$ together with the slowing down time $\tau_0 = 97$ ms (only i-i collisions are relevant) the triton density is $n_t = 7.7 \cdot 10^{13}$ $m^{-3}$. Taking again the volume at ½ plasma radius to be filled with tritons the neutron production rate comes out to be

$$R_{14MeV} = n_t n_p (\sigma v)_0 \cdot Vol = 2.9 \cdot 10^{13} s^{-1}.$$

Hence, the 14 MeV neutron rate is at least 200 times below the 2.5 MeV neutron rate and can therefore be neglected in the neutron calculations.

Table II. Neutron production and operation scenario for various experiments

| | FTU | | Tore Supra | Asdex-UP | W 7-X |
|---|---|---|---|---|---|
| | refer. scen. | 2. oper. scen. | | | |
| n/shot | $6.0 \cdot 10^{16}$ | | $2.0 \cdot 10^{17}$ | $5.0 \cdot 10^{16}$ | $6.0 \cdot 10^{16}$ |
| shots/hour | 4 | 4 | | | |
| shots/day | | | 10 | 50 | 10 |
| hours/day | 9 | 8 | | | |
| days/year | | | | 4 | 50 |
| days/week | 4 | 5 | 5 | | |
| weeks/year | | 9.375 | 12 | | |
| weeks/month | 3 | | | | |
| months/year | 7 | | | | |
| shots/year | 3024 | 1500 | 600 | 200 | 500 |
| n/year | $1.8 \cdot 10^{20}$ | $9.0 \cdot 10^{19}$ | $1.2 \cdot 10^{20}$ | $1.0 \cdot 10^{19}$ | $3.0 \cdot 10^{19}$ |

The operation scenarios and the annual production of 2.5 MeV neutrons at W 7-X are compared to the projected data of the tokamak experiments ASDEX-Upgrade, Tore Supra[5], and FTU[6]. Table II shows a survey of the shots and the produced neutrons. Fig. 3 shows the time history of the different operation scenarios and

[5] C.Diop, M.Chatelier, G.Brandicourt, C.Cladel, G.Ermont, A.Le Dieu De Ville, C.Lyraud, J.C.Nimal, Les Risques Radiologiques Autour De Tore Supra, DRFC-SCP, Lab. Report EUR-CEA-FC-1164 (1982)

[6] Frascati Tokamak Upgrade, ENEA Frascati, Lab. Report 82.49 (1982)

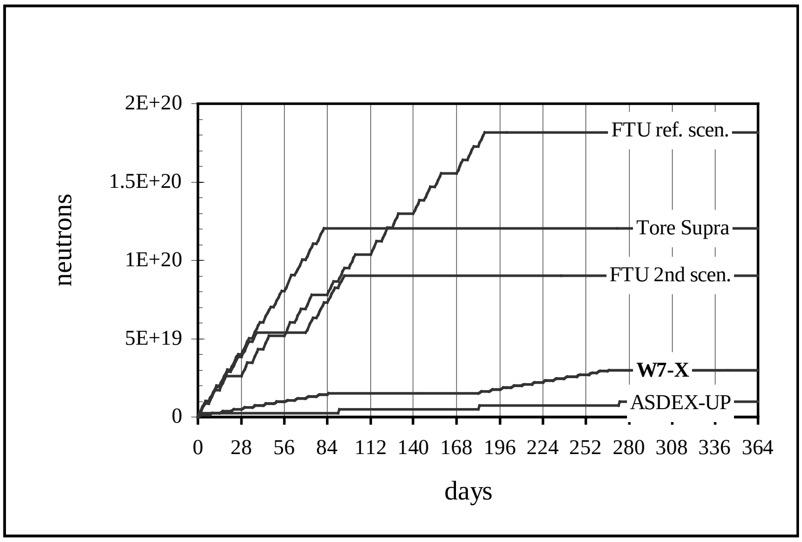


Figur 3. Neutron production scenarios for a one year period of various experiments. The number of neutrons produced by W 7-X is three times that of ASDEX-Upgrade.

neutron productions. ASDEX-Upgrade will produce almost the same number of neutrons per shot as W 7-X, but the annual rate will be 3 times less because of the lower number of pulses per year. Tore Supra is expecting a 4 times higher number of neutrons per year than for W 7-X. For FTU, the number of neutrons is expected to be even 3 to 6 times higher than that expected for W 7-X, depending on the scenario.

# Neutron Transport

The monoenergetic neutrons from the plasma interact with all the surrounding material. These collisions lead to scattering, energy loss, and absorption of the neutrons. This fairly complex transport problem has been studied in different approaches. The deterministic method leads to the problem of solving a singular integro differential equation[7,8,9,10,11,12,13]. This is most commonly solved by the multigroup discrete ordinate method. ANISN[14,15] is one of the available numerical codes which solves the problem for anisotropic scattering but only for the simple one-dimensional geometry. This approach is well suitable for plane, cylindrical, and spherical symmetric geometries.

The tokamak both with circular as well as with D-shaped cross section has been fairly well approximated[16,17]. The stellarator geometry however is far to complex to be described with these methods in any detail.

In contrast to the deterministic method, the neutron transport problem for more than one dimension and for the full energy distribution of the neutrons can be solved by statistical methods using random numbers to determine the outcome of each individual collision. The probability distributions are randomly sampled at each event using the appropriate cross-section for energy loss, scattering and absorption.

## Monte Carlo Code MCNP

The Monte Carlo code MCNP (Monte Carlo Neutron Particle)[18] solves the coupled transport of neutrons and photons through any complex three-dimensional geometry. Starting from an arbitrary three-dimensional neutron source, the neutron flux, the energy spectrum, the thermal power deposition, and the dose rate can be evaluated anywhere in space. Nuclear reactions lead to the generation of photons whose transport is solved simultaneously. In addition to this MCNP evaluates the activation of the material by neutron collisional reactions. The extensive library ENDF/B-VI provides pointwise cross-section data. A collection of variance reduction techniques is used to improve the statistical accu-

7 M.C. Case, P.F. Zweifel, Linear Transport Theory, Addison-Wesley Publ. Comp., Reading, Mass. (1967)
8 E.E. Lewis, W.F. Miller jr., Computational Methods of Neutron Transport, John Wiley & Sons, N.Y. (1984)
9 H. Greenspan, C.N. Kelber, D. Okrent (Ed‘s.), Computing Methods of Neutron Transport, Gordon and Breach Sc. Publ., N.Y. (1984)
10 M. Akiyama (Ed.), Design Technology of Fusion Reactors, World Scientific, Singapore (1991)
11 P.F. Zweifel, Reactor Physics, McGraw-Hill Comp. (1973)
12 G.I. Bell, S. Glasstone, Nuclear Reactor Theory, Van Norstrand Reinold Comp., N.Y. (1970)
13 W. Roos, Analytic Functions and Distributions in Physics and Engineering, John Wiley & Sons, N.Y. (1969)

14 W.W. Engle, Jr., A Users Manual for ANISN, A One Dimensional Discrete Ordinates Transport Code With Anisotropic Scattering, Oak Ridge National Laboratory, Lab. Report K-1693 (1967)
15 L.P. Ku, J. Kolibal, ANISN/PPL-C, A One Dimensional Multigroup Discrete Ordinates Code, A User’s Guide, PPPL, Princeton University, EAD-R-11 (1982)
16 U.Fischer, Die neutronenphysikalische Behandlung eines (d,t)-Fusionsreaktors nach dem Tokamakprinzip (NET), Lab. Report KfK 4790 (1990)
17 G.Fieg, Monte Carlo Calculations with the MCNP Code for Investigations of Neutrons and Photon Transport at the ASDEX Upgrade Tokamak, Lab. Report KfK 4851 (1991)
18 J.F. Briesmeister (Ed.), MCNP – A General Monte Carlo N-Particle Transport Code, Version 4B, LA-12625-M, Manual (1997)

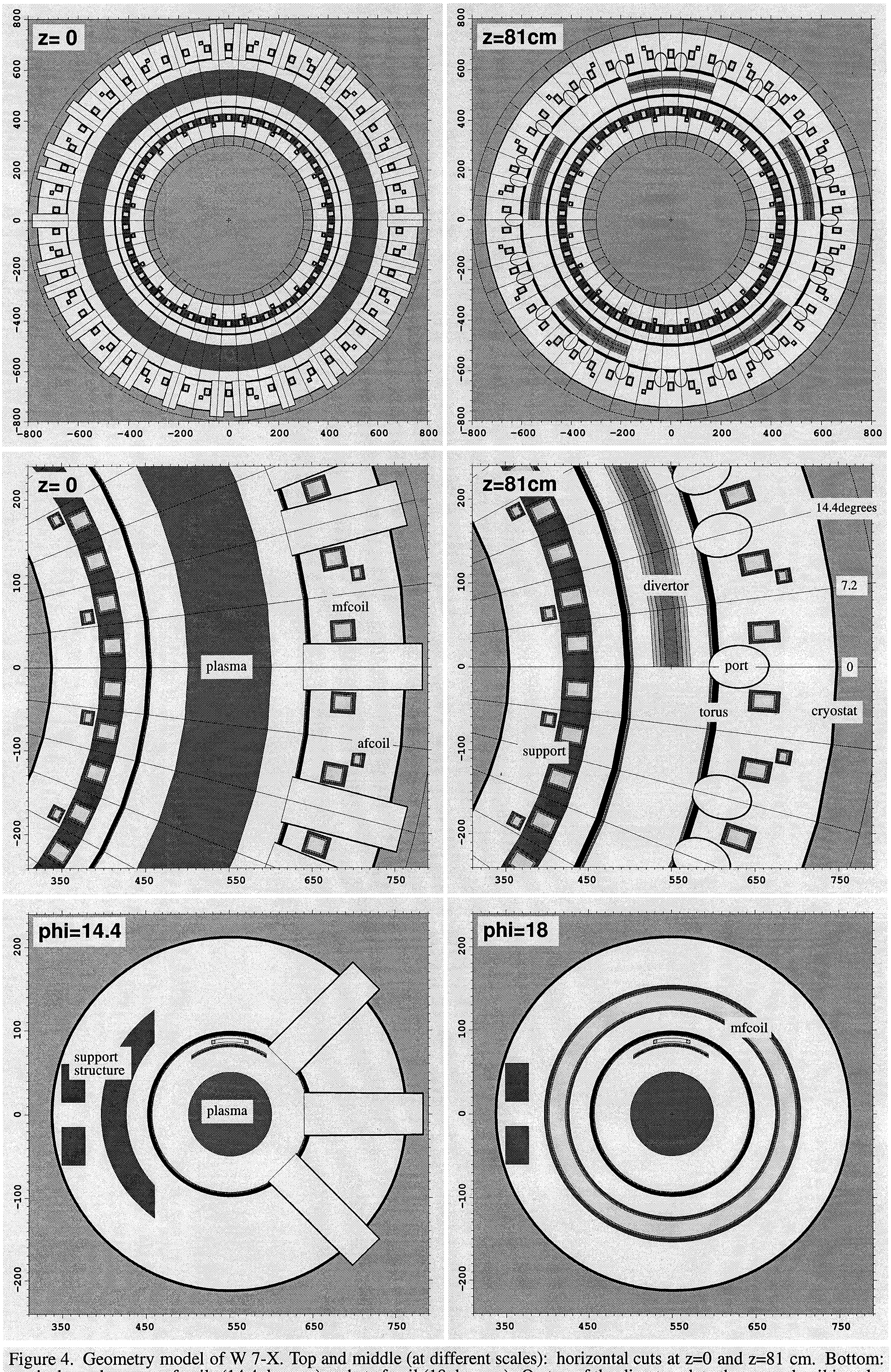


Figure 4. Geometry model of W 7-X. Top and middle (at different scales): horizontal cuts at z=0 and z=81 cm. Bottom: vertical cuts between af coils (14.4 degrees) and at af coil (18 degrees). On top of the divertor plate the control coil is to be seen. Details of the geometry, the masses and the densities are described at the appendix and the mcnp input file.

racy. The most recent release MCNP4B has been used for the evaluations of this report.

## Modelling of W 7-X

The geometry input for MCNP asks for the full three-dimensional space subdivided into cells which are individually bounded by a set of surfaces. Each individual cell can be filled homogeneously with the desired material or a composition of several materials or nothing, i.e. vacuum. For modelling W 7-X, the only cell bounding surfaces used are planes and cylinders. The complicated geometry of the torus has been simplified by using a circular torus with a circular cross-section. This is almost perfectly approximated by 50 cylindrical sections. The same simplification holds for the cryostat which encloses all the coils. The 50 twisted modular field (mf) coils and the 20 tilted auxiliary field (af) coils are all simplified by plane and circular coils oriented perpendicularly to the equatorial plane. The collection of very different ports has been simplified by modelling cylindrical ports for $\theta = 0$, $+ 45°$, $- 45°$. These simplifications have very little effect on the fluxes and spectra outside the structure. Inside the structure, however, closer to the plasma neutron source, and in particular at the first wall the inhomogeneities and effects of flux and power peaking of the neutron load (very important for the reactor) cannot be described correctly by this model. The adequate description of the three-dimensional shape of the torus and the coils demands more effort to set up this complicated geometrical input file for MCNP.

The major dimensions of the real experimental set-up have been taken exactly wherever possible. Dimensions like the torus radius or the wall radius which show a substantial variation both in toroidal and in poloidal direction have been replaced by appropriate averaged values. The thickness of closed material shields, like torus and cryostat, have been kept correctly in order not to disturb their shielding and thermalizing effects on the outgoing neutrons. A marginal discrepancy of up to 10% between the real masses and the masses taken for the simplified geometrical model has been tolerated.

The geometry model as used for the MCNP calculations is shown in Fig. 4. The top pictures show a horizontal cut of the full torus at z = 0 (equatorial plane) and at z = 81 cm (cut through the divertor plates). An enlarged view of these cuts is seen on the pictures in the middle of Fig. 4 which show several details like the composition of the mf coils and the af coils. The bottom pictures show vertical cuts through the ports and through the mf coil. The coils are modelled by the rectangular packet of superconductor surrounded by fiberglass epoxy and the steel housing. The torus, the cryostat, the ports, and the coils are all covered with copper sheets on their cold surfaces which work as the heat shields. The inside wall of the torus is plated with graphite tiles and copper underneath for the mechanical support of the graphite. Further details like the divertor and the control coils behind the divertor plates are described in the appendix. The mechanical support structure is simulated by two closed circular steel rings at the inboard side of the coils and wedge shaped spacers from steel between the coils. The dimensions of the support structure is adjusted to get the real weight correctly. The number and the aperture of the ports are adjusted to represent the sum of the apertures of all the real ports.

All the geometrical details as well as the density and the composition of the materials are descibed in the appendix which in particular contains the complete

Table III. Weight of materials (in tons) of all machine components.

| total weight of components [t] | | SS 1.4429 | SS 1.4311 | Cu heat shield | Cu plates | super conductor | fiberglass epoxy | graphite tiles | solder | TZM | water | air |
|---|---|---|---|---|---|---|---|---|---|---|---|---|
| mf coils | 188.67 | 110.00 | | 6.57 | | 54.30 | 17.80 | | | | | |
| af coils | 32.52 | 20.90 | | 1.83 | | 5.96 | 3.86 | | | | | |
| torus | 77.33 | | 59.90 | 1.74 | 11.60 | | | 4.09 | | | | |
| cryostat | 99.41 | | 95.50 | 3.91 | | | | | | | | |
| support | 125.00 | 125.00 | | | | | | | | | | |
| ports | 20.86 | 18.30 | | 2.56 | | | | | | | | |
| control coils | 0.55 | 0. 13 | | | 0. 42 | | | | | | | |
| divertor | 6.36 | | | | 2.64 | | | 0.82 | 0.052 | 2.52 | 0.33 | |
| exp. hall 24 000 $m^3$ | 31.20 | | | | | | | | | | | 31.20 |
| total weight of material [t] | 581.9 | 274.33 | 155.40 | 16.61 | 14.66 | 60.26 | 21.66 | 4.91 | 0.052 | 2.52 | 0.33 | 31.20 |

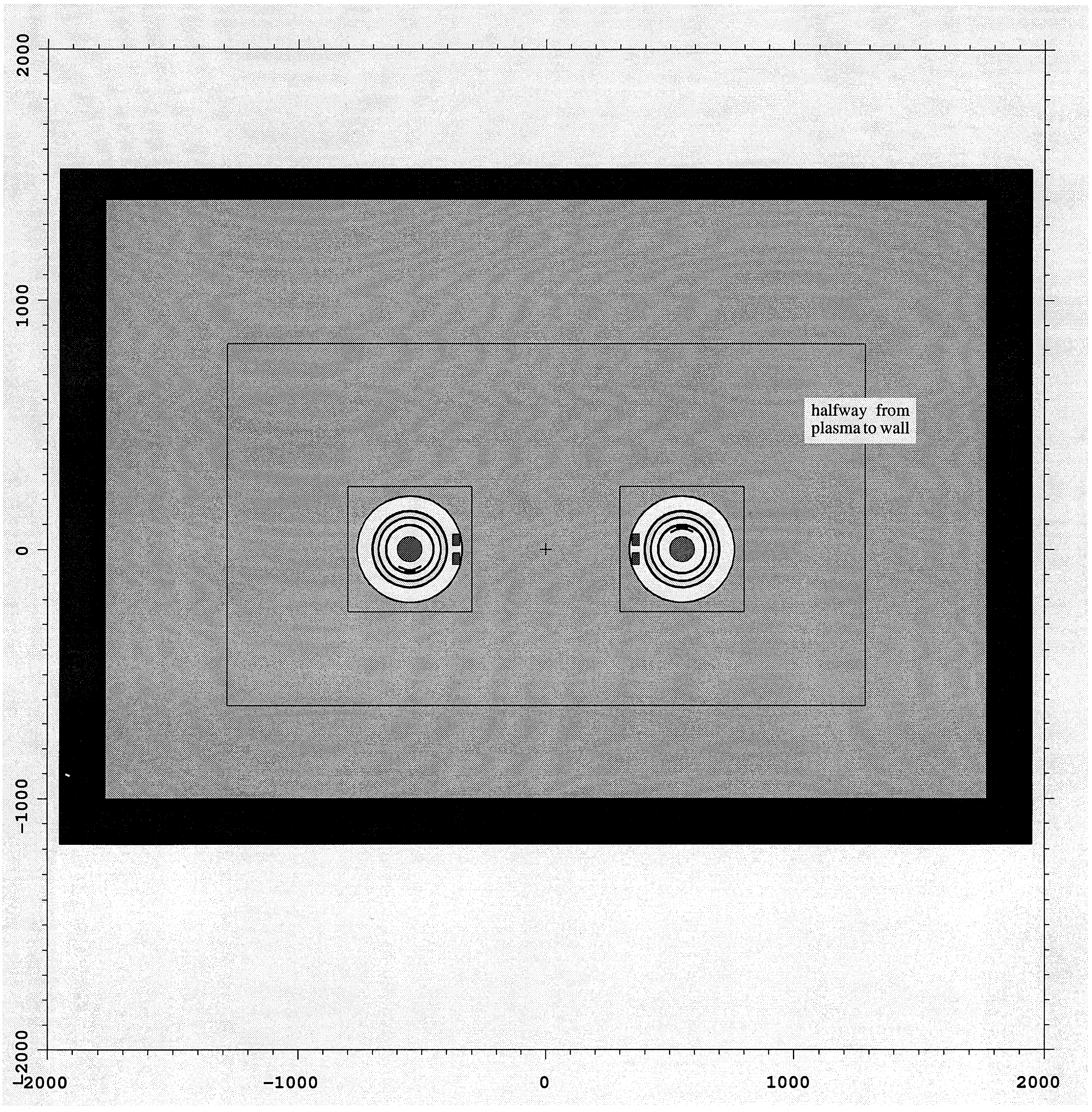


Figure 5. Geometry model of the experimental hall and the experiment W 7-X. The hall (rectangular in reality) is modelled by a cylinder of 24m hight (real hight) and 17.7m radius (adjusted to get the real volume of 24 000 cubicmeters) at the inside. The walls, the floor and the roof are build from borated concrete. The thickness is 1.8m for the walls and the floor and 1.2m for the roof.

Table IV. Weight of chemical elements (in tons) of all machine components.

| | H | C | N | O | Na | Mg | Al | Si | Ar | Ca | Ti | Cr | Mn | Fe | Co | Ni | Cu | Zr | Nb | Mo | Ag |
|---|---|---|---|---|---|---|---|---|---|---|---|---|---|---|---|---|---|---|---|---|---|
| mf coils | 0.53 | 5.49 | | 5.84 | 1.03 | 0.71 | 25.3 | 3.26 | | 1.37 | 2.13 | 19.35 | 2.20 | 71.30 | 0.006 | 14.30 | 26.93 | 0.06 | 5.85 | 3.03 | |
| af coils | 0.11 | 1.19 | | 1.27 | 0.22 | 0.11 | 2.79 | 0.68 | | 0.30 | 0.23 | 3.67 | 0.42 | 13.54 | 0.001 | 2.72 | 4.07 | 0.01 | 0.64 | 0.57 | |
| torus | | 4.09 | | | | | | | | | | 10.78 | 1.20 | 41.92 | 0.003 | 5.99 | 13.34 | | | | |
| cryostat | | | | | | | | | | | | 17.19 | 1.91 | 66.83 | 0.005 | 9.55 | 3.91 | | | | |
| support | | | | | | | | | | | | 21.88 | 2.50 | 80.91 | 0.007 | 16.25 | | | | 3.44 | |
| ports | | | | | | | | | | | | 3.20 | 0.37 | 11.84 | 0.001 | 2.38 | 2.56 | | | 0.50 | |
| control coils | | | | | | | | | | | | 0.07 | 0.01 | 0.27 | 0.000 | 0.05 | 0.13 | | | 0.01 | |
| divertor | 0.04 | 0.82 | | 0.29 | | | | | | | 0.003 | | | | | | 2.65 | | | 2.52 | 0.039 |
| exp. hall 24 000 $m^3$ | | | 23.6 | 7.24 | | | | | 0.406 | | | | | | | | | | | | |
| total weight of element [t] | 0.68 | 11.6 | 23.6 | 14.6 | 1.25 | 0.82 | 28.1 | 3.95 | 0.406 | 1.67 | 2.37 | 76.14 | 8.60 | 286.6 | 0.022 | 51.24 | 53.59 | 0.06 | 6.49 | 10.07 | 0.039 |

input file for the MCNP programme. Table A-I at the appendix lists the dimensions, the volumes, and the masses of all machine components as being used for the MCNP input file. A summary of the weight of the machine components and of all the different materials of these components is given in Table III. From this it is obvious that most of the steel is concentrated at the support structure, the mf coil housings and the cryostat (331 tons of totally 430 tons). The torus consists of 60 tons of steel. The other main weight contributions are the NbTi superconductor (60 tons) which is embedded into fiberglass epoxy (22 tons), and the copper heat shield and the copper support structure (31 tons) for the graphite tiles (5 tons). The experimental hall is filled with air (31 tons). Alltogether, including the air, the experiment weighs 582 tons. Table IV lists the chemical constituents of the machine components. It will turn out that the 54 tons of Cu, 76 tons of Cr, 287 tons of Fe, and 22 kg of Co will become most important for the short, medium, and long term activation.

For the MCNP input file maximum use has been made of the symmetry and the periodicity of the W 7-X experiment. Five identical modules build up the full torus and each module has a 180° rotational symmetry around a horizontal axis oriented radially through the middle of the module. Therefore only one half of a module needs to be modelled in all details. This half module ranges from 0° to 36° in toroidal direction. It is composed of 136 cells which are bounded by 110 surfaces (planes and cylinders). A rotational transformation by 180° around the symmetry axis of the module completes a full module from one half module and five rotational transformations by multiples of 72° around the vertical axis through the center of the experiment complete the full torus from one full module.

## Modelling of Experimental Hall

The experimental hall in reality has a rectangular shape. Starting from the middle of the W 7-X experiment the distances to the walls are -16.2 m and +16.2 m in one horizontal direction (west to east) and -17.2 m and +13.2 m in the other horizontal direction (south to north). The distance to the ground floor is -9.3 m and to the roof +14.7 m. The walls and the floor are build from borated concrete with a concentration of 700 ppm of B. The thickness of the walls is 1.8 m and the thickness of the roof and the ground floor is 1.2 m. At -5.5 m, below the equatorial plane of the experiment, there is an intermediate floor of 0.40 m borated concrete with a central circular hole of 4.0 m diameter.

For the MCNP calculations this hall is modelled simply by a circular cylinder with the roof at the top and the ground floor at the bottom. The intermediate

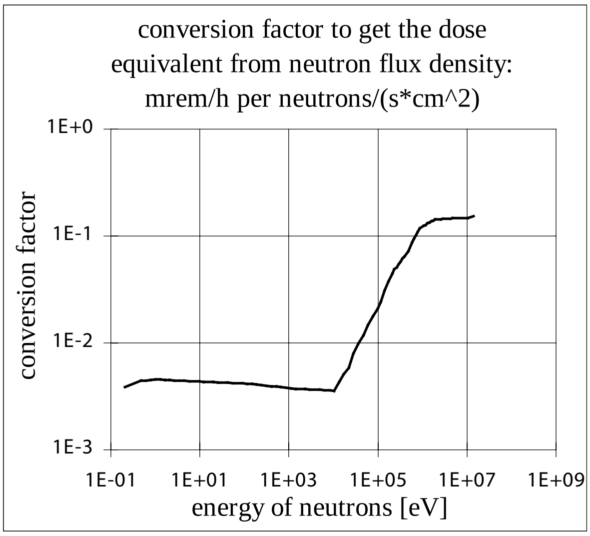


Figure 6. Neutron flux conversion to dose rate.

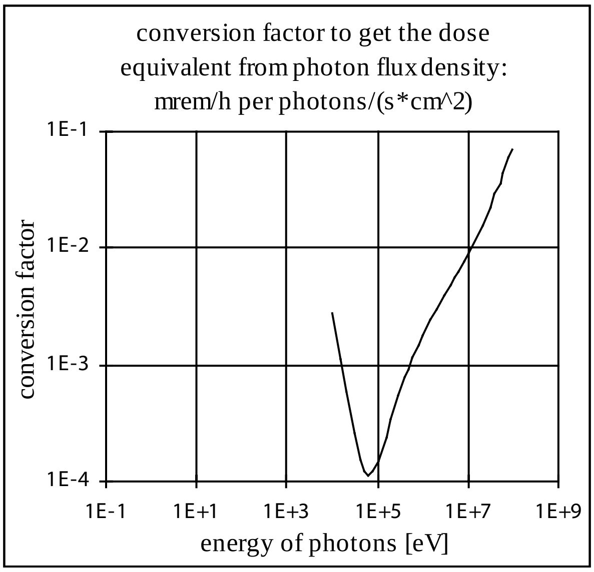


Figure 7. Photon flux conversion to dose rate.

floor has been omitted. The hight of 24.0 m is taken like the real distance from the floor to the roof and the radius of 17.7 m is taken to keep the inside volume of the hall correctly to 24 000 $m^3$. Fig. 5 shows the experimental hall with the W 7-X experiment. A cylinder whose wall, top, and bottom are halfway between the experiment and the hall indicates the position where neutron flux calculations are taken representative for the inside of the hall.

# Fluxes and Dose Rates

The source of neutrons is assumed to be a circular line source positioned at the plasma center. This simplification neglects any nonuniformities near to the plasma and the torus. Outside the experimental structure, at all places inside the hall and, in particular, outside the concrete shielding walls, this simplification is of no importance. The primary neutrons at 2.5 MeV, by scattering with the surrounding material, loose their energy and get thermalized, produce photons by nuclear reactions, or get absorbed. The MCNP code takes all these collisional interactions into account and also follows the tracks of the photons including their scattering and absorption processes. The cross-sections for all the different elements and processes as needed for the materials of W 7-X are available from the ENDF/B-VI library. The dose rates both from the neutron fluxes and from the photon fluxes can easily be evaluated by the code using the appropriate conversion factors[19,20,21] as shown in Figs. 6 and 7.

As described before the annual averaged rate of $1 \cdot 10^{12}$ n/s is taken for all the following calculations of fluxes and dose rates.

## Inside the Experimental Hall

Inside the experimental hall, surrounded by concrete walls, the fluxes of neutrons and photons are of particular importance for the diagnostic equipment which is sensitive to this radiation and, not being shielded, might be distorted. Therefore, the flux of neutrons as well as photons normalized to the energy interval of 1 MeV and the unit area of 1 $cm^2$ is calculated together with their energy distributions at the following positions:

- **inside of torus**, i.e. at the inside wall surface of the steel torus which is at a distance of 95 cm from the plasma center,
- **outside of cryostat**, i.e. at the surface of a torus enclosing all the toroidal structure with a squared cross-section of 500 cm x 500 cm,
- **middle of hall**, i.e. on a cylindrical surface halfway between the experiment and the walls, the roof and the floor,
- **at wall of hall**, i.e. on the inside surface of the concrete walls, roof and floor.

The flux spectra at these four postions have been calculated taking into account the influence of the surrounding walls, the floor, and the roof. Fig. 8 and Fig. 9 show the neutron flux spectra (on double logarithmic scale) for normal concrete and for borated concrete. The corresponding photon flux spectra (logarithmic flux scale and linear energy scale) are shown on Fig. 10 and Fig. 11.

For normal concrete (Fig. 8) the fast neutrons (2.5 MeV) are 100 times less frequent in the middle of the hall compared to the inside of the torus. From the outside of the cryostat to the wall, the flux of fast neutrons drops by a factor of 5 due to the dilution by the increasing distance from the source. This fast neutron flux at the wall is 2 times higher than expected from the geometrical dilution factor of about 10. A substantial fraction of the fast neutrons is scattered back from the walls. The flux of thermal neutrons fills the hall

[19] Recommendations of the International Commission on Radiological Protection, ICRP Publications 15 and 21, Pergamon Press (1978)
[20] see: Manual ANISN
[21] Normenausschuss Radiologie im DIN (Deutsches Institut fuer Normung), DIN 6802, Tabelle 3 (1978)

very homogeneously like a thermal gas. Even inside the torus, this thermal flux is already half as high as inside the hall.

Doping the concrete of the walls, the floor, and the roof with 700 ppm of Boron (B) has no effect at all on the flux at all energies inside the torus (Fig. 9) as this flux is determined purely by the collisional interaction with the surrounding material close to the plasma. Outside the torus, i.e. at all positions inside the hall, the flux of the fast neutrals is also not affected by the B. This is expected as B only absorbs the thermal neutrons. The B doping works most effectively on the thermal flux inside the hall which drops substantially, by a factor of 30. This reduction of the thermal neutron flux inside the hall will become very important for the Ar activation of the air.

For normal concrete the photon flux (Fig. 10) at all energies is a factor of 10 to 20 higher inside the torus compared to the hall. From the outside of the cryostat towards the wall, the photon flux falls down not more than a factor of 3. This shows the important role of the walls for the photon production. A substantial fraction of the photons inside the hall is produced by the collisional interaction of the neutrons with the wall materials. The shape of the spectrum is due to the specific nuclear reactions of the neutrons with the materials that are very different at the torus and at the concrete walls. The flux inside the hall is almost homogeneous. Only outside the cryostat the photon flux increases by about a factor of 2 for low photon energies and up to a factor of 5 for high photon energies. Inside the hall six pronounced lines show up at 2.3, 3.5, 4.9, 6.3, 7.3, and 7.7 MeV. These lines are not seen inside the torus.

Doping the walls with 700 ppm of B has no effect at all on the photon

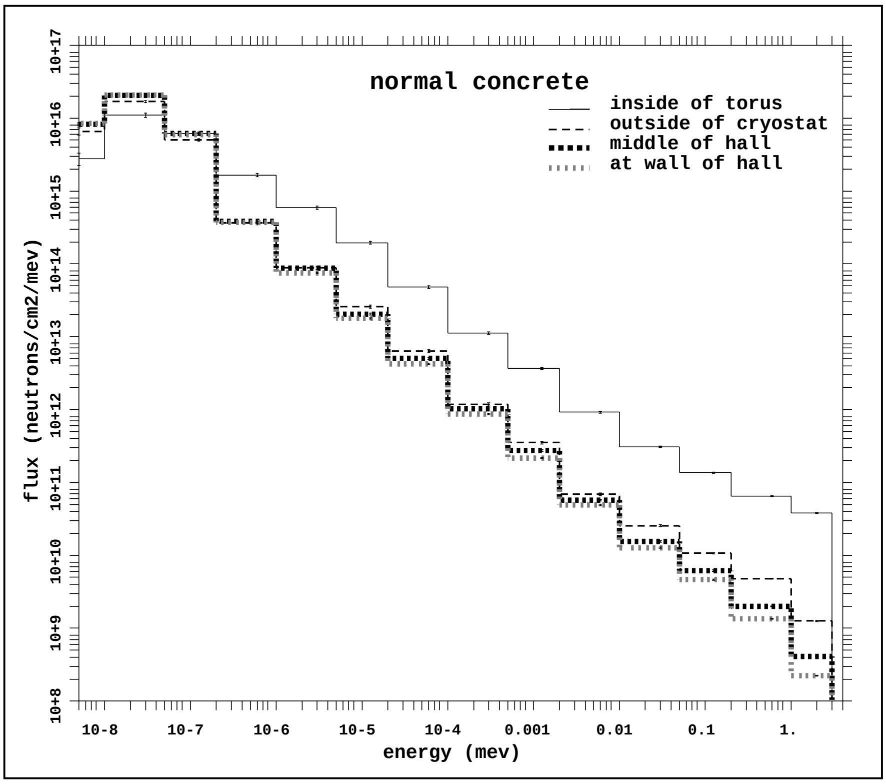


Figure 8. Neutron flux at different surfaces for normal concrete walls. Thermal neutron flux is lowest inside the torus. Fast neutron flux decreases with the distance from the source.

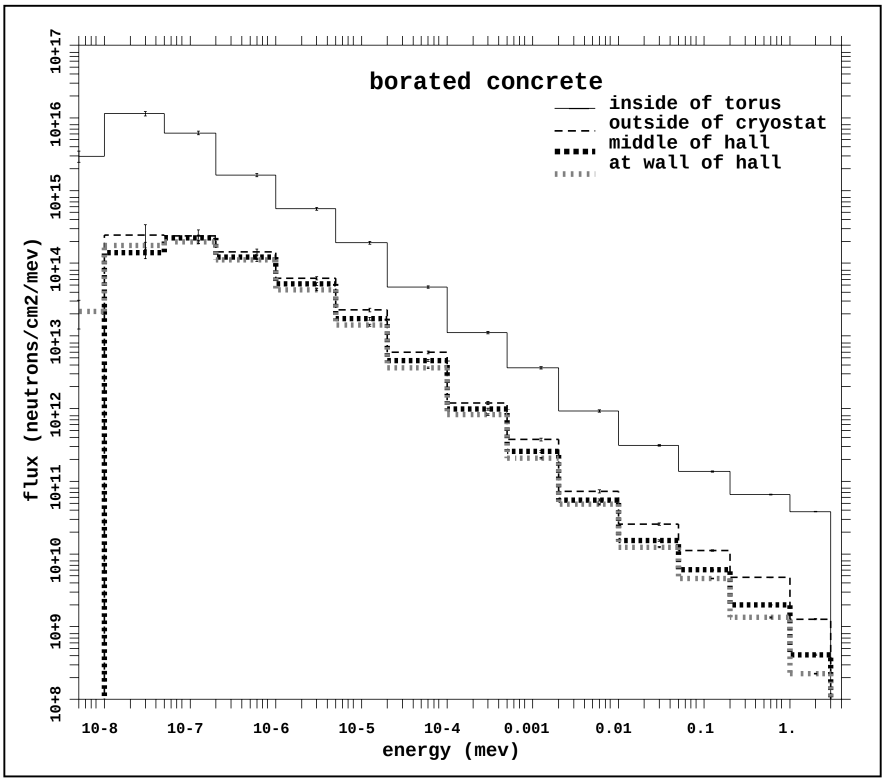


Figure 9. Neutron flux at different surfaces for borated concrete walls. Thermal neutron flux inside the hall is lowered by a factor of 30. The fast neutron flux is unaffected by the B.

flux inside the torus (Fig. 11). But outside the torus, the photon flux above 1 MeV is substantially lower, a factor of 2 outside the cryostat and up to a factor of 5 at the wall. This obviously is due to the B doping and the resulting reduction of the flux of thermal neutrons which largely contribute to the photon generation. The spectral shape is much the same as without B. The lines, seen with normal concrete, have disappeared quantitatively except one line at 7.5 MeV.

## Shielding by the Walls

The pulse scenario as described generates $3 \cdot 10^{19}$ neutrons/year which means $10^{12}$ neutrons/s for the annual averaged flux. Expanding into free space, not taking the interaction with any material into account, this annual averaged neutron flux converted into the annual dose equivalent leads to $3.5 \cdot 10^5$ mSv/year at a distance of 17 m from the plasma. This is the typical distance between the plasma and the shielding wall of the experimental hall. The legal regulations allow 0.3 mSv/year only for biological safety reasons. Therefore, the shielding of a concrete wall has to be large enough to reduce the dose rate by the large factor of more than $10^6$.

To study the shielding properties of a concrete wall, the very primitive geometrical model of a point source surrounded by a spherical concrete wall starting at a radius of 17 m has been chosen. The dose rate by the neutrons as well as by the photons is plotted in Fig. 12 on the inside surface of the wall and on Fig. 13 on the outside surface of the wall. The thickness of the wall was gradually increased by adding slices of 5, 10, and 25 cm of concrete to the foregoing concrete wall. By MCNP the fluxes of the neutron and the photons were calculated and converted to the annual dose equivalent. As the overall result it comes out that a 2 m

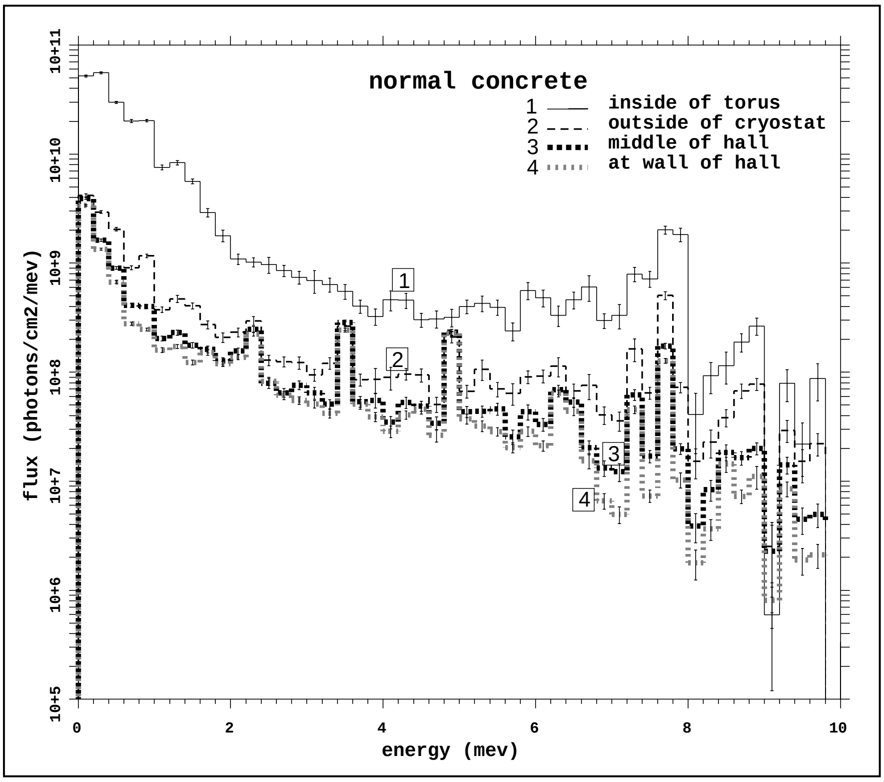


Figure 10. Photon flux at different surfaces for normal concrete walls. Flux is highest inside the torus and almost homogeneous inside the hall. Lines occur at 2.3, 3.5, 4.9, 6.3, 7.3, and 7.7 MeV.

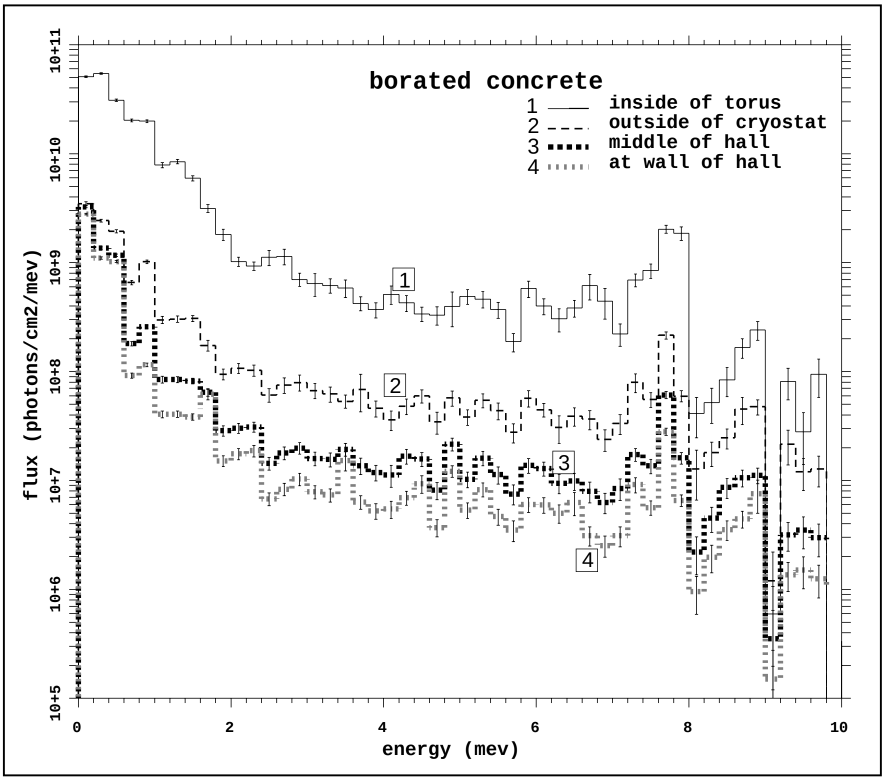


Figure 11. Photon flux at different surfaces for borated concrete walls. Inside the torus the flux is unaffected by the B. The lines have disappeared and the flux is lowered inside the hall.

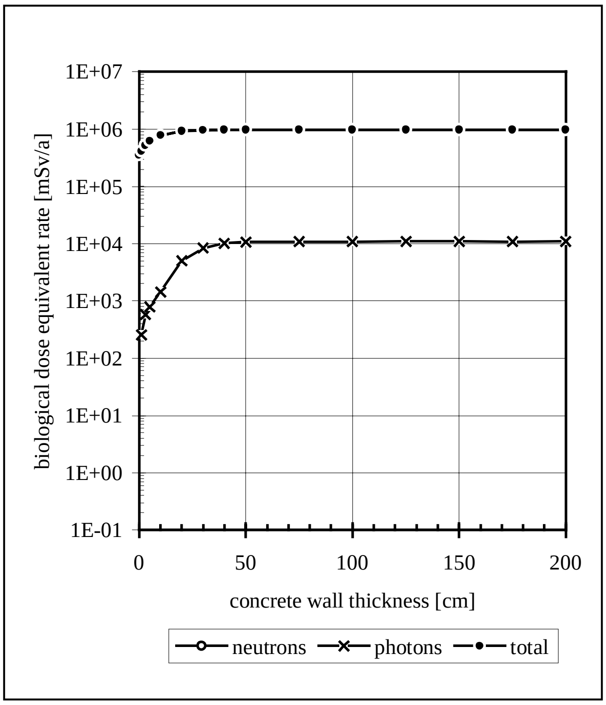


Figure 12. At the inside of a concrete wall of more than 30 cm thickness the neutron induced dose rate is 100 times higher than the photon induced dose rate.

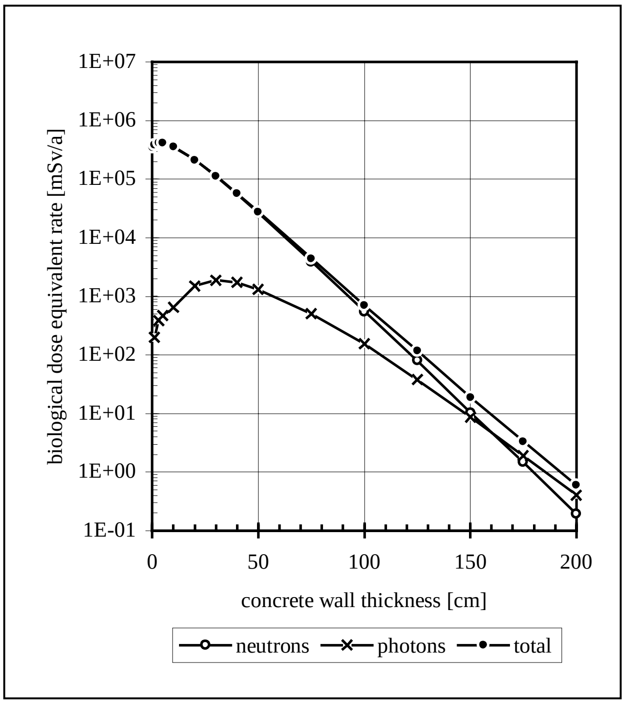


Figure 13. At the outside of a concrete wall the photon induced dose rate becomes higher than the neutron induced dose rate for a wall of more than 160 cm thickness.

thick ordinary concrete wall will provide sufficient shielding.

At the inside of the wall (Fig. 12) the neutron induced dose rate is responsible for the total dose rate. For a wall up to 20 cm, the albedo of the neutrons first increases the dose rate at the inside wall surface. Having started at $3.5 \cdot 10^5$ mSv/year the dose rate almost triples and saturates at $9.6 \cdot 10^5$ mSv/year. As a secondary effect, by nuclear reactions, the neutrons produce photons whose dose rate increases with the thickness of the wall. At a wall thickness 40 cm this photon induced dose rate saturates at 1% of the neutron induced dose rate.

At the outside surface of the wall (Fig.13), the neutron induced dose rate, after a slight increase with the wall thickness up to 10 cm falls exponentially with the increasing wall thickness. The photon induced dose rate starting from nothing reaches a maximum of $2.0 \cdot 10^3$ mSv/year for 30 cm wall thickness which is 0.2% of the neutron induced dose rate at this wall thickness. Increasing the width of the wall, both dose rates finally decay exponentially for walls over 1 m width. Photons are absorbed less effectively than neutrons. At 1.6 m both dose rates are equal, and for 2 m the photon induced dose rate already dominates. Any additional need for biological shielding should deal

Table V. Different concrete mixtures differ by their absorption length $d_{1/100}$ from 63.5 cm to 55.0 cm.

| | | concrete mixture from mcnp manual (la) | | normal concrete NB 1 from Sauermann Table 7 | | normal concrete 100 l water/m^3 from DIN 25431 | |
|---|---|---|---|---|---|---|---|
| | density = | 2.251 | $g/cm^3$ | 2.386 | $g/cm^3$ | 2.300 | $g/cm^3$ |
| | atomic weight | density contrib. $g/cm^3$ | weight-% | density contrib. $g/cm^3$ | weight-% | density contrib. $g/cm^3$ | weight-% |
| H | 1.008 | 0.010 | 0.453 | 0.013 | 0.545 | 0.011 | 0.490 |
| B | 10.811 | | | | | | |
| C | 12.011 | | | | | 0.127 | 5.540 |
| **O** | 15.999 | 1.154 | **51.260** | 1.165 | **48.826** | 1.127 | **49.000** |
| Na | 22.991 | 0.026 | 1.155 | 0.040 | 1.676 | | |
| Mg | 24.312 | 0.009 | 0.387 | 0.060 | 2.515 | | |
| Al | 26.981 | 0.080 | 3.555 | 0.107 | 4.484 | 0.019 | 0.820 |
| **Si** | 28.086 | 0.811 | **36.036** | 0.730 | **30.595** | 0.496 | **21.550** |
| S | 32.064 | | | 0.003 | 0.126 | | |
| K | 39.102 | 0.032 | 1.422 | 0.045 | 1.886 | | |
| Ca | 40.080 | 0.098 | 4.355 | 0.194 | 8.131 | 0.474 | 20.600 |
| Fe | 55.847 | 0.031 | 1.378 | | | 0.046 | 2.000 |
| Ni | 58.710 | | | 0.029 | 1.215 | | |
| Ba | 137.340 | | | | | | |
| | total = | 2.251 | 100.00 | 2.386 | 100.00 | 2.300 | 100.00 |
| | $d_{1/100}$ = | **63.5** | cm | **57.5** | cm | **55.0** | cm |

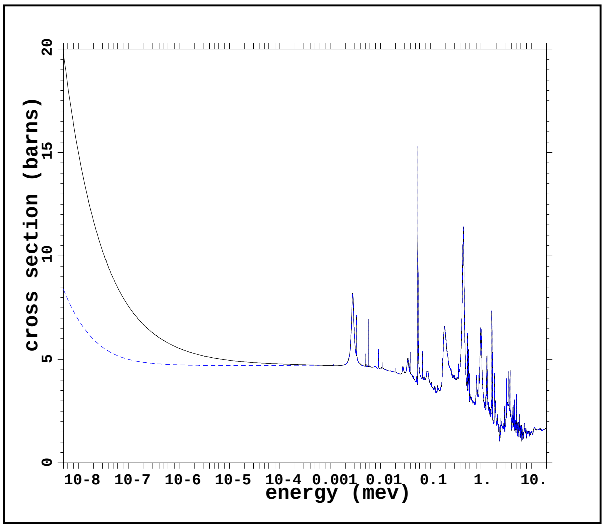


Figure 14. For the normal concrete (lower curve) the cross-section for thermal neutrons is at least 2 times lower than that for the borated concrete (upper curve).

preferentially with the reduction of the photon flux rather than the neutron flux.

All these calculations hold for ordinary concrete. The composition of this concrete is listed in the left column of Table V and taken from the MCNP manual. This type of concrete has also been used for the wall shielding calculations for the ASDEX-Upgrade experiment. The total cross-section of this concrete for neutrons is shown on the lower curve at Fig. 14. The upper curve shows the cross section for borated concrete with 700 ppm B. This B concentration easily increases the total collisional cross section of ordinary concrete by a factor 2 for the thermal neutrons. Other types of concrete have also been considered. The two types, normal concrete NB1[22] (middle column) and normal concrete with 100 l water/m$^3$ from DIN 25431 (right column), have similar compositions as that of the Los Alamos type. The shielding capability, however, expressed as the width of the wall which reduces the total dose rate by a factor 100, varies mainly in dependence on the density. The figures for $d_{1/100}$ at Table V, last line, show that a wall which reduces the dose rate by the desired factor of $10^6$ might vary in width by 25 cm depending on the composition of the concrete.

The neutron absorption can be substantially improved by adding B to the concrete mixture. This is due to the very large absorption cross-section of B for thermal neutrons. Transport calculations with a doping of 700 ppm of B show a dose reduction of about a factor 4 at the outside of the wall. The resulting width reduction of the wall comes very close to 20 cm. This improvement of the shielding already saturates at 600 ppm of B. Increasing the B concentration beyond this value has almost no additional shielding effect.

The actual design for the W 7-X experimental hall is based on calculations with normal concrete including 100 l water/m$^3$ from DIN 25431 which is doped with 1 000 ppm of B. A width of 1.80 m of this type of concrete keeps the total dose rate below the biological safety limit of 0.3 mSv/year. The calculations carried out by the GRS (Gesellschaft für Reaktorsicherheit at Garching) have taken into account the real structure of the experimental hall, including the intermediate floor, and modelling also the ducts for the heating installations for ECRH, ICRH, NI, and also for the cryoinstallations.

## Skyshine

The concrete surrounding the whole experiment (walls, roof and floor) has a characteristic shielding length of $d_{1/100} < 60$ cm. Therefore, the dose rate on top of the 120 cm thick roof is more than 100 times larger than the dose rate at the outside of the 180 cm thick walls. It has been calculated how large the dose rate due to skyshine, i.e the backscatter of neutrons from the air, will be at the fence outside the hall.

For the skyshine model, the hall is surrounded by air with a water content of 10 g per 1 kg of air up to a distance of 300 m. The fence is assumed to be at 100 m distance from the experiment. To reduce the variance

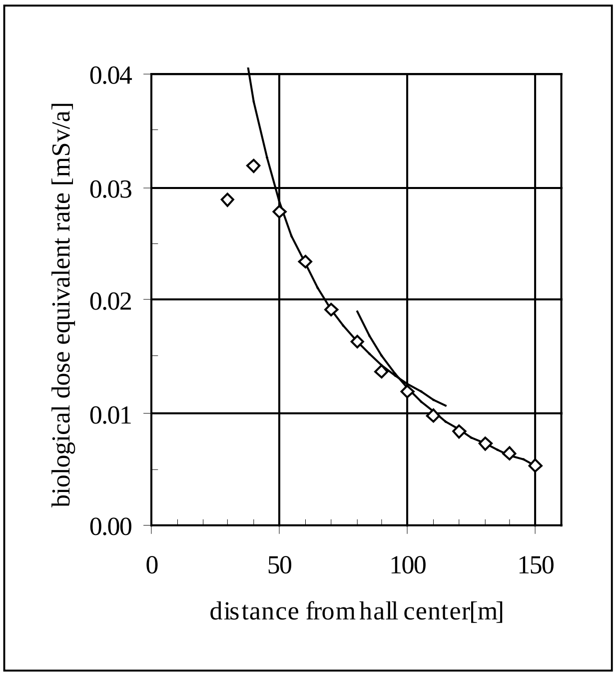


Figure 15. The skyshine of the neutrons leads to a dose rate which falls like $R^{-1/2}$ up to 100 m and like $R^{-2}$ above 100 m distance from the center of the hall.

[22] P.F.Sauermann, Radiation Protection by Shielding, K.H. Thiemig Munich, Table 7, p. 50 (1976)

of the statically evaluated results MCNP has the facility of the ring detector which collects a flux contribution from each individual collision anywhere in space taking into account the attenuation factor for the materials on the straight line between the point of collision and the position of the ring detector. This ring detector has been placed at radial distances from 30 to 150 m from the experiment. The neutron induced dose rate in dependence on the distance is seen in Fig. 15. Varying the radius of the ring detector from 30 to 150 m, the dose rate decreases like $R^{-1/2}$ up to 100 m and like $R^{-2}$ for larger radii. In the very near region of less than 40 m where the distance to the wall is of the order of the wall dimensions, the skyshine is partly shadowed by the wall. Only a reduced part of the sky can be "seen" by the ring detector. Therefore, the dose rate even drops very close to the wall. The backscatter of neutrons from the sky at the distance of 100 m leads to a dose rate of only 0.01 mSv/year which is 30 times lower than the legally tolerated dose rate. The photon backscatter by the air affects the dose rate at the distance of 100 m by only a few percent of the dose rate by the backscattered neutrons.

If the dose rate at the outside of the walls is simply lowered by the factor 30, which is the squared increase of the radial distance from the wall at 17 m to the fence at 100 m, the resulting dose rate is the same as the calculated skyshine at the fence. At the fence at 100 m from the source the dose rate by the direct fluxes (neutrons and photons) is only doubled by the effect of the skyshine of the neutrons.

# Neutron Induced Activation

The collisional interaction of neutrons with atoms leads to an activation of many materials of the experimental structure. From the biological safety point of view this neutron induced activation is not negligible for the W 7-X experiment. The emitted radiation will have to be monitored during the time the experiment is running and also for some length of time after any sequence of pulses. The dominant process for material activation is neutron capture by the reaction path (n,γ). Only for fast neutrons (2.5 MeV) the reaction path (n,p) becomes important. The number of atoms activated by $6 \cdot 10^{16}$ neutrons, i.e. the number of neutrons released by one 10 s pulse, has been calculated by the MCNP code taking the cross-sections for the appropriate reaction paths for all the different materials. The activity, i.e. the number of the activated atoms divided by the half life period, dies away after each experimental pulse, during the breaks between the various pulse sequences, and after the end of the total lifetime. This intermittent pulse scenario has been taken into account to evaluate the time history of the activity of each constituent of the different materials. The activation of the machine structure and the activation of the air are described in the following two chapters.

## Activation of the Structure Material

For the investigation of the experimental structure, the following materials have been considered: stainless steel (SS 1.4429 and SS 1.4311), copper, superconductor compound (NbTi, Cu, Al, fiberglass epoxy), solder,

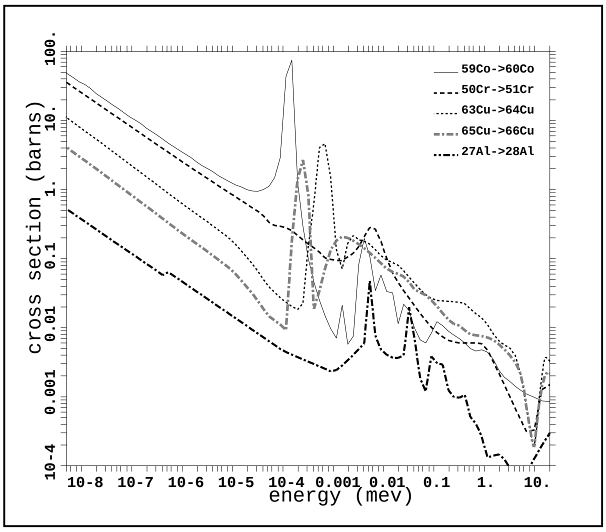


Figure 16. Cross-sections for (n, γ) reactions follow 1/velocity for thermal energies and show strong resonances for epithermal and fast neutrons.

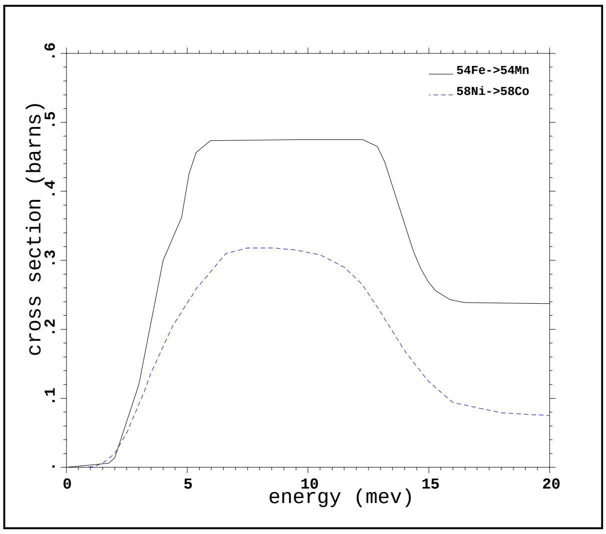


Figure 17. Cross-sections for (n, p) reactions are negligibly low below 1 MeV and show sharp increase above 2 MeV.

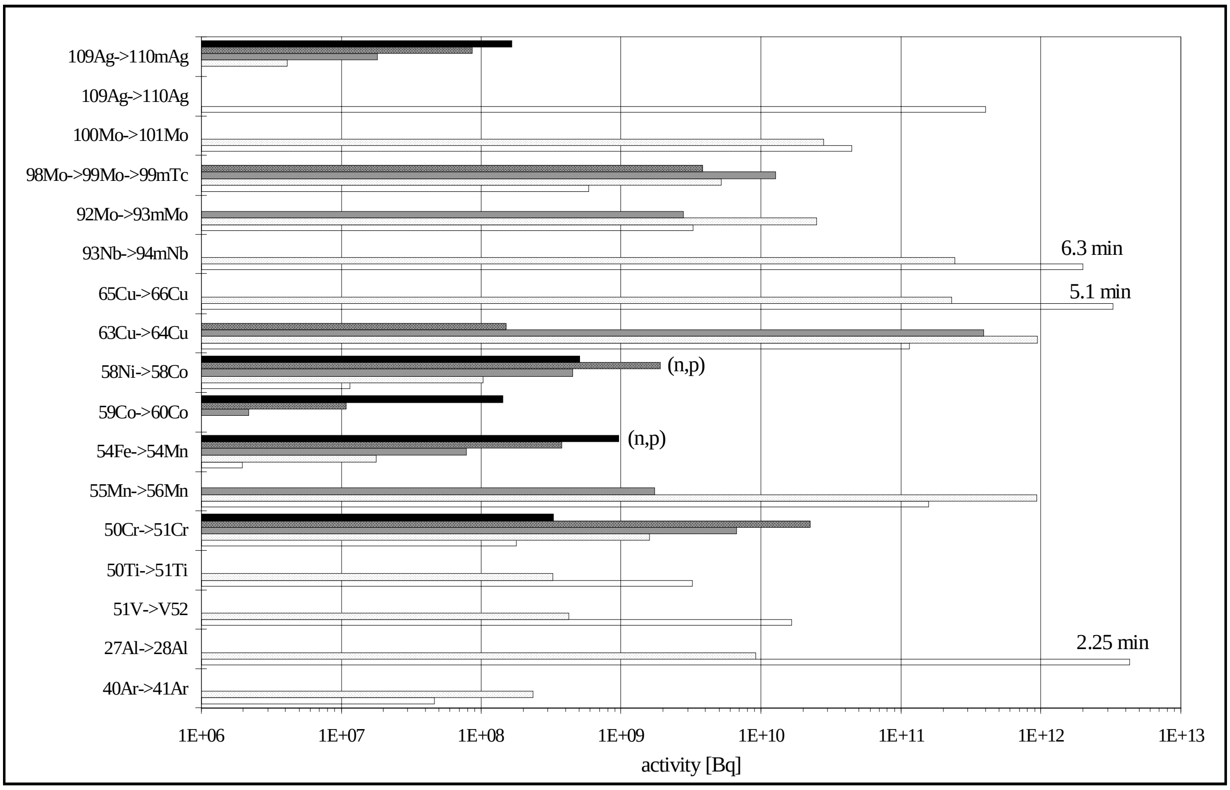


Figure 18 a. Incremental activities not having waited for any cooling time. $^{28}Al$, $^{66}Cu$, and $^{94}Nb$ are the most dominant isotopes at the short timescale (minutes).

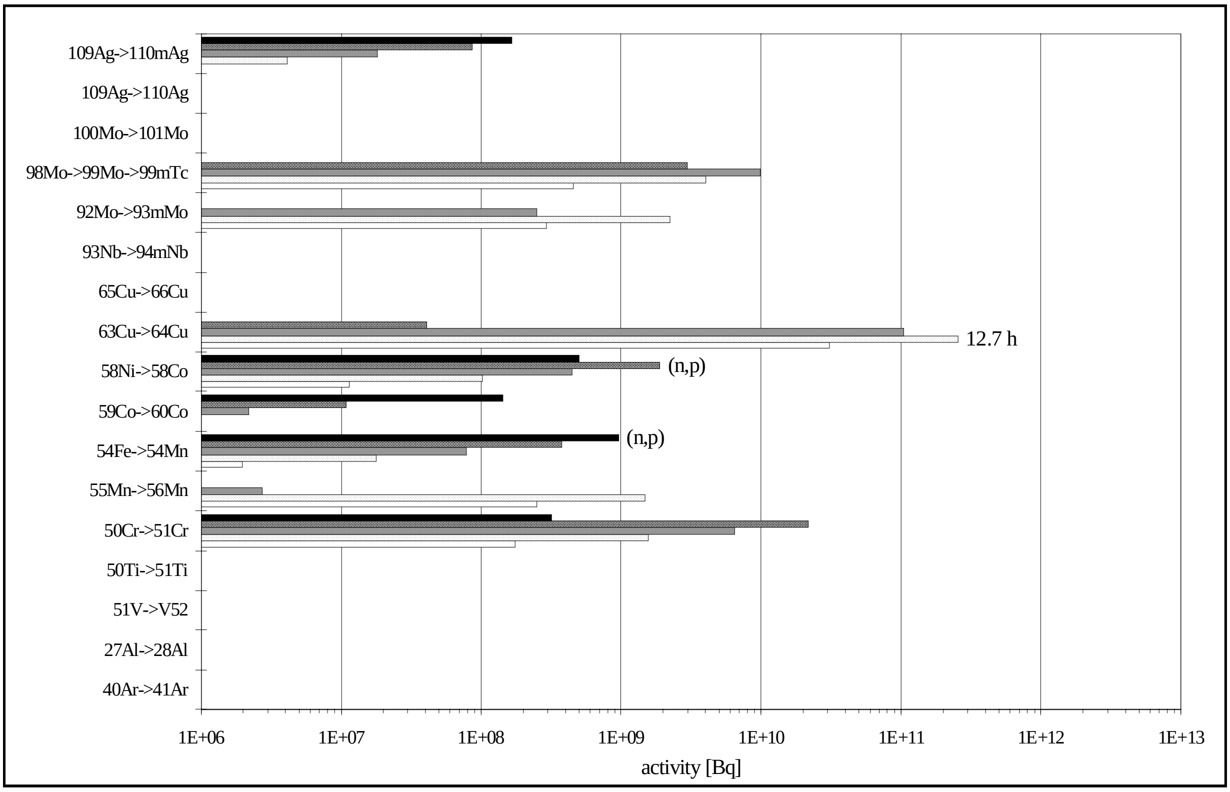


Figure 18 b. Incremental activities after having waited for **1 day** of cooling time. $^{64}Cu$ is the most dominant isotope at the medium timescale (hours) .

**Figure 18. Activities immediately after one pulse (bottom bar = 1st bar) and the incremental activities, i.e. additional activities, produced by one series (2nd bar), one period (3rd bar), one campaign (4th bar), and the lifetime (5th bar = top bar) for all activated elements.**

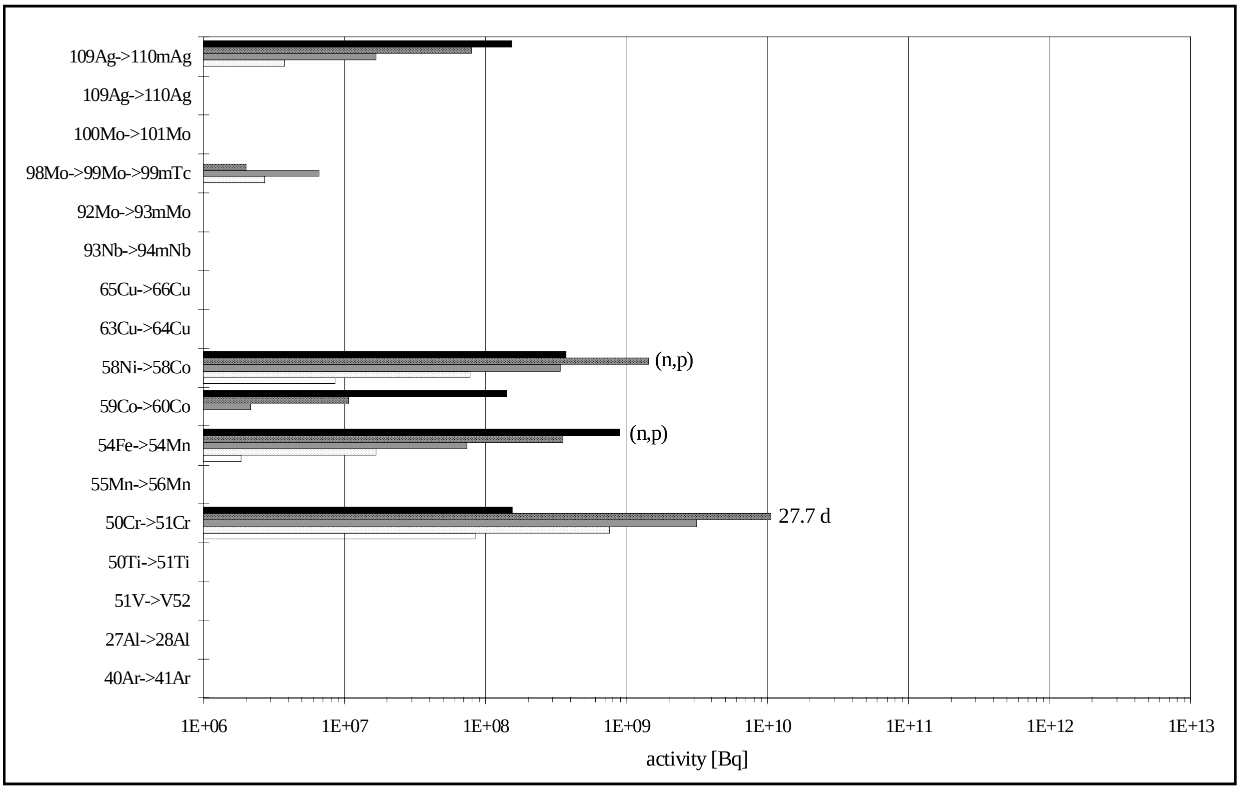


Figure 18 c. Incremental activities after having waited for **1 month** of cooling time. $^{51}Cr$ is the most dominant isotope at the long timescale (days).

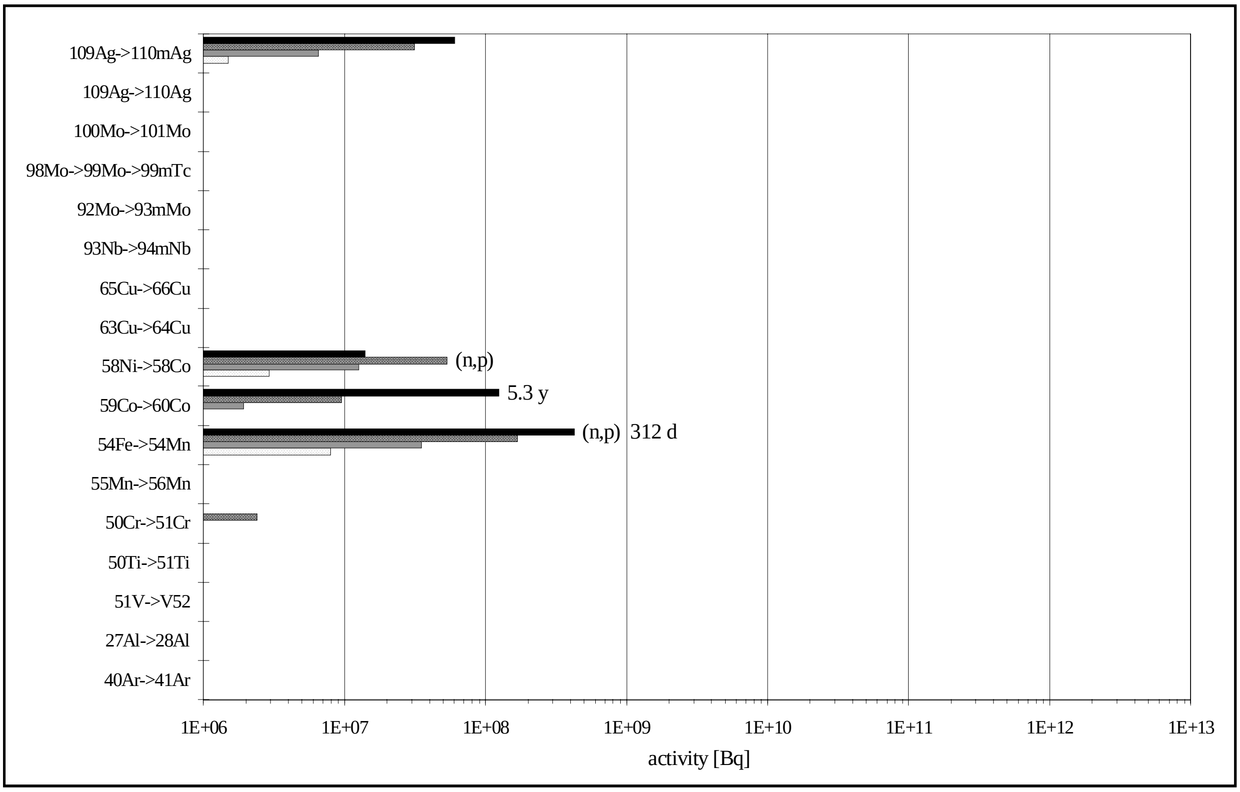


Figure 18 d. Incremental activities after having waited for **1 year** of cooling time. $^{54}Mn$ is the most dominant isotope at the very long timescale (months) .

**Figure 18 (contd.). Activities immediately after one pulse (bottom bar = 1st bar) and the incremental activities, i.e. additional activities, produced by one series (2nd bar), one period (3rd bar), one campaign (4th bar), and the life-time (5th bar = top bar) for all activated elements.**

and tzm. The composition of these materials by the different elements together with their physical constants and their resulting number of atoms per barn·cm as needed for the calculations by the MCNP code are listed in Table A-II at the appendix. Some activation cross-section plots are shown at Fig. 16 and Fig. 17. Fig. 16 shows the cross-sections for the (n,γ) activation of $^{59}Co$, $^{50}Cr$, $^{63}Cu$, $^{65}Cu$, and $^{27}Al$, all of which follow the 1/velocity law for low energies up to $10^{-4}$ MeV. The activation cross-section for Co is larger than all the others. Many resonances occur for the epithermal and the fast neutrons.

Very differently, Fig. 17 shows that the cross-sections for the (n,p) activation of $^{54}Fe$ and $^{58}Ni$, which convert to the isotopes $^{54}Mn$ and $^{58}Co$, start to become relevant only just below the starting energy of 2.5 MeV of the emitted neutrons.

The total activities of all the activated elements are shown in Figs. 18 a-d. The bars show by the bottom bar for each element the activity due to a single pulse only. The subsequent bars on top of the bottom bar represent the incremental activities due to the quoted sequence of pulses not counting for the activity produced by the last pulse or the by the preceding sequence or sequences of pulses. Thus, the summary of all five bars gives the total activity after the last pulse of the lifetime of the experiment. The four figures represent the activities immediately after the last pulse (Fig. 18 a), after one day (Fig. 18 b), after one month (Fig. 18 c), and after one year (Fig. 18 d) of cooling time. The maximum activities in dependence on the cooling time are directly correlated to the half life period of the different isotopes.

- Immediately after the last pulse of any sequence of pulses, the activity is dominated by the short living isotopes $^{28}Al$, $^{66}Cu$, and $^{94m}Nb$, with $T_{1/2}$ = 2.25, 5.1, and 6.3 min (Fig. 18 a).

Waiting for various lengths of cooling time after a single pulse or after any sequence of pulses, different isotopes contribute most to the activity:

- After one day of cooling time (Fig. 18 b) $^{64}Cu$ with $T_{1/2}$ = 12.7 h activated to a maximum by a 10 pulse series,
- after one month of cooling time (Fig. 18 c) $^{51}Cr$ with $T_{1/2}$ = 27.7 days activated to a maximum by a 5 day period,
- and after one year of cooling time (Fig. 18 d) $^{54}Mn$ with $T_{1/2}$ = 312 d from the 10 years lifetime.
- Waiting for five years after the end of the lifetime of the experiment, the only activity left is that from the long living $^{60}Co$ isotope with $T_{1/2}$ = 5.3 years.

Summing up the activities of all elements leads to the time history shown in Fig. 19. This total activity never supersedes $1.2 \cdot 10^{13}$ Bq and decays down to $2.6 \cdot 10^{9}$ Bq between the ½ year campaigns. The residual activity of $1 \cdot 10^{8}$ Bq at 5 years after the lifetime follows the exponential decay of $^{60}Co$ for the subsequent time.

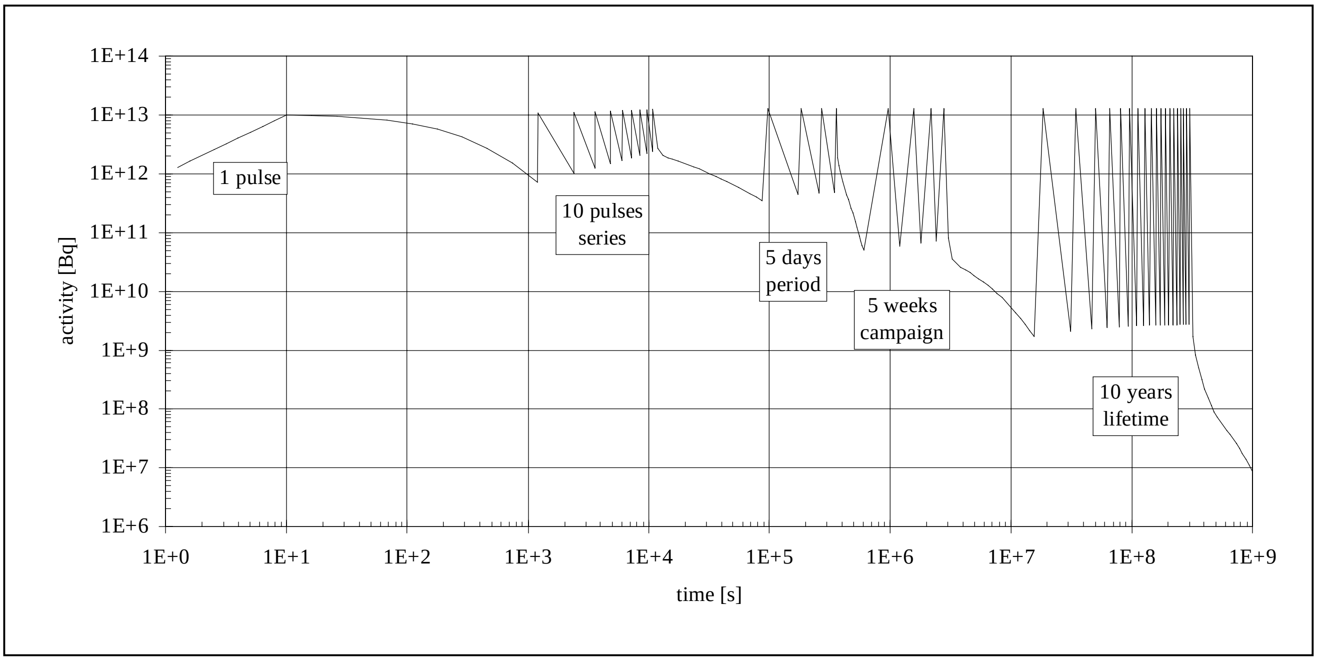


Figure 19. Time history of the total activity summarized over all radioactive constituents of the experiment. The decay periods reflect the pulse scenario over the 10 years lifetime.

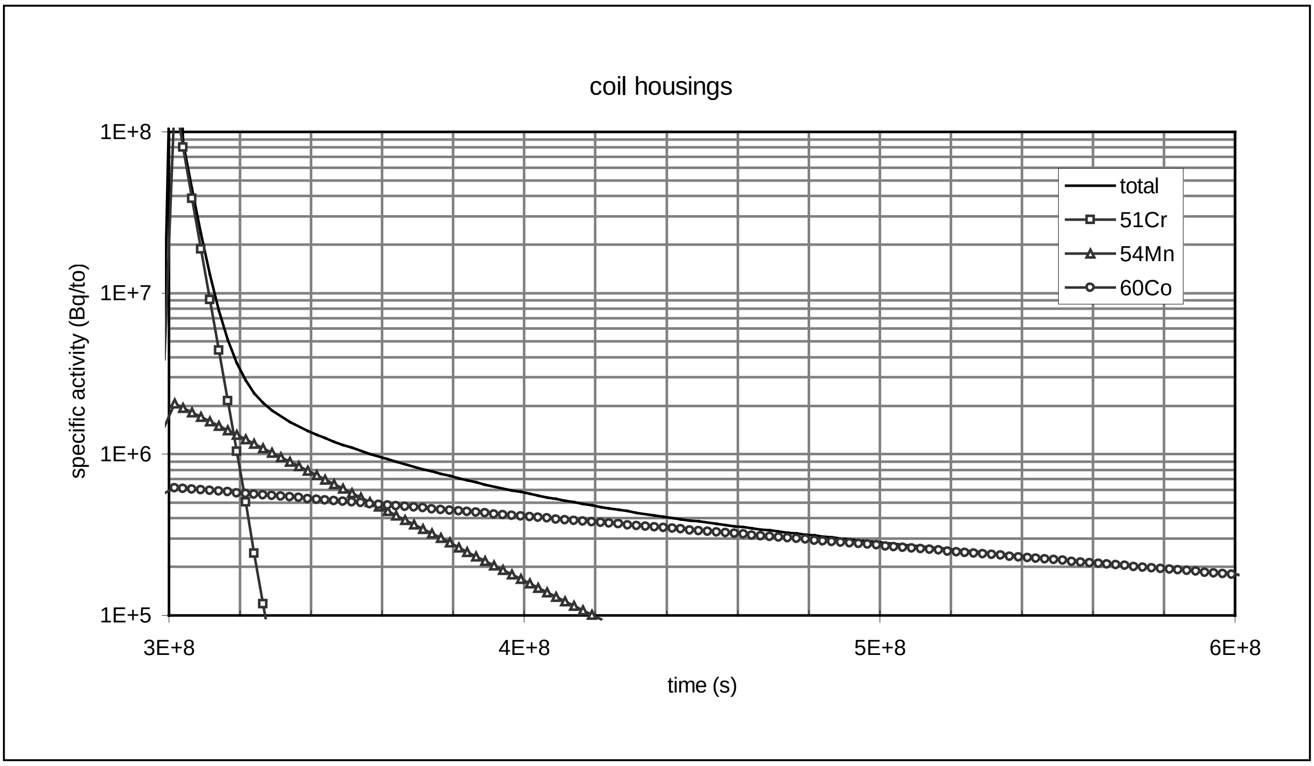


Figure 20. Specific activity (Bq/to) of the steel of the coil housings. From $3.6 \cdot 10^8$ s onwards, which is 1.85 years after the shutdown of the experiment, $^{60}$Co becomes the dominant isotope.

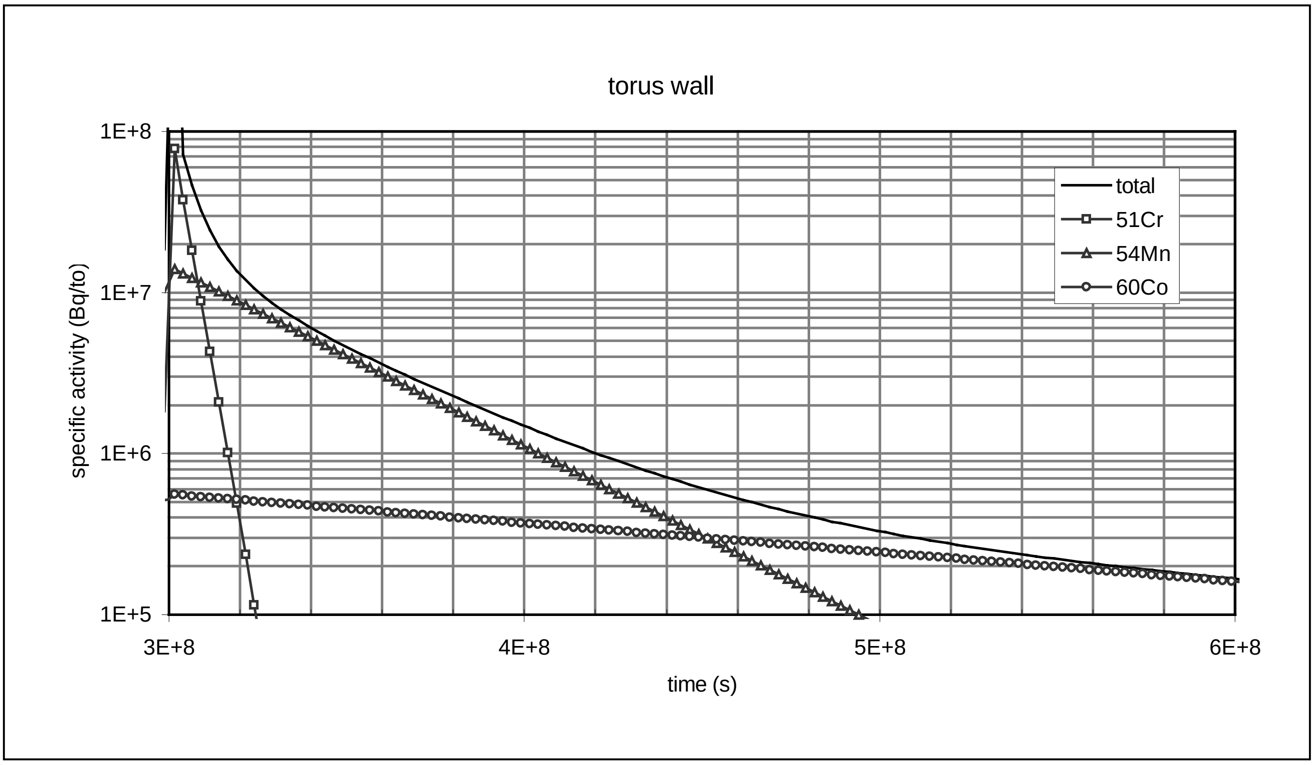


Figure 21. Specific activity (Bq/to) of the torus wall. From $4.5 \cdot 10^8$ s onwards, which is 4.8 years after the shutdown of the experiment, $^{60}$Co becomes the dominant isotope.

## Long Term Deactivation

On the time sale of minutes and hours the superconductor compound together with the copper heat shields determine the total activity by the isotopes $^{28}$Al, $^{94}$Nb, and $^{66}$Cu. On the longer time scale of months and years, however, the steel components only cause the residual activity. Depending on the time scale the dominant radioactive isotopes change from $^{51}$Cr to $^{54}$Mn and to $^{60}$Co.

After shut down, the end of the lifetime of the experiment, the deactivation of the steel components has been considered in some detail. For the problem of decommissioning and transportation of the materials the specific activity, which is the activity per unit weight of the component under consideration (Bq/to), rather than the total activity is the relevant quantity which has been evaluated for the following. Fig. 20 and Fig. 21 show the specific activity of the most important steel components, the coil housings and the torus wall, for the time from the shut down (= $3.02 \cdot 10^8$ s) up to 10 years of cooling time.

Fig. 20 shows the specific activity of the steel housings of all the 50 mf and 20 af coils. Up to 8 months $^{51}$Cr is the dominant isotope. At this time $^{54}$Mn shows the same specific activity and stays to be dominant until 1.8 years. From that time onwards $^{60}$Co becomes the only isotope left which contributes to the total activity of the coil housings.

Fig. 21 shows the specific activity of the torus wall which is different to that of the coil housings. The $^{51}$Cr and the $^{60}$Co activities are somewhat less but the $^{54}$Mn activity is substantially higher than those of the steel housings. This is because inside the torus the thermal neutron flux, responsible for the Cr and Co activation, is somewhat lower. In contrast to this the $^{54}$Mn isotope is produced by the fast neutrons. And these are already substantially moderated after having passed through the torus wall. Again, up to 7 months $^{51}$Cr is the dominant isotope. But $^{54}$Mn stays to be dominant for a longer time. At 4.8 years $^{60}$Co takes over the role of the dominant isotope.

The support structure and the cryostat wall show less specific activity compared to the coil housings: 2 times less for $^{54}$Mn, 3 to 4 times less for $^{60}$Co, and 8 times less for $^{51}$Cr. The reason for this is the flux dilution by the larger distance from the neutron source and the spacial variation of the neutron spectrum.

The total specific activities, i.e. the summation of the specific activities of all the steel constituents, have been compared for the different components and for various cooling down times after the lifetime. Having taken the activation and decay for the pulse scenario into account the result as shown at Table VI is the following:

Table VI. Total specific Activities Bq/to after the experimental lifetime of 10 years having waited afterwards for various cooling down times. The dominant isotopes change from $^{51}$Cr to $^{54}$Mn and to $^{60}$Co.

| specific activities Bq/to of steel components | | | | |
|---|---|---|---|---|
| | weight | 1 month | 1 year | 10 years |
| torus wall | 60 to | $4.7 \cdot 10^7$ | $\mathbf{9.0 \cdot 10^6}$ | $\mathbf{1.5 \cdot 10^5}$ |
| coil housings | 131 to | $\mathbf{9.8 \cdot 10^7}$ | $1.3 \cdot 10^6$ | $\mathbf{1.7 \cdot 10^5}$ |
| support structure | 125 to | $1.3 \cdot 10^7$ | $6.8 \cdot 10^5$ | $5.7 \cdot 10^4$ |
| cryostat | 96 to | $1.2 \cdot 10^7$ | $7.2 \cdot 10^5$ | $4.2 \cdot 10^4$ |
| dominant isotopes: | | **$^{51}$Cr** | **$^{54}$Mn** | **$^{60}$Co** |
| half life period: | | 27.7 days | 312.2 days | 5.272 years |

- The coil housings and the torus wall dominate the activity for all times after the lifetime. The support structure and the cryostat show less and about equal activities for all times.
- After one month of cooling time the dominant isotope is $^{51}$Cr which shows a maximum of $9.8 \cdot 10^7$ Bq/to at the coil housings and half of this at the torus wall. The other components have about 7 times less activity.
- After one year of cooling time, the dominant isotope is $^{54}$Mn which shows a maximum of $9.0 \cdot 10^6$ Bq/to at the torus wall. The coil housings have already 7 times less activity compared to the torus wall. The other steel components have about 13 times less activity compared to the torus wall.
- After 10 years of cooling time, $^{60}$Co is the only radioactive isotope left. Torus wall and coil housings show an activity of 1.5 to $1.7 \cdot 10^5$ Bq/to. At the support structure and the cryostat the activity is 3 to 4 times less.

The long living $^{60}$Co causes no problems after having waited for about 10 years after shut down of the experiment. The remaining specific activities are all well below $1 \cdot 10^6$ Bq/to at which level a recycling of the steel as scrap material can be allowed by the legal regulations. The residual activity is even close to $1 \cdot 10^5$ Bq/to at which level it can be allowed to freely use the steel for any further fabrication.

## Activation of the Air

The flux of thermal neutrons inside the experimental hall has a high probability to activate the argon by the reaction $^{40}Ar(n,\gamma)^{41}Ar$. The cross-section for this activation shows exactly the 1/velocity dependence up to the MeV range in contrast to the collisional cross-section which is almost constant (see Fig. 22). The number

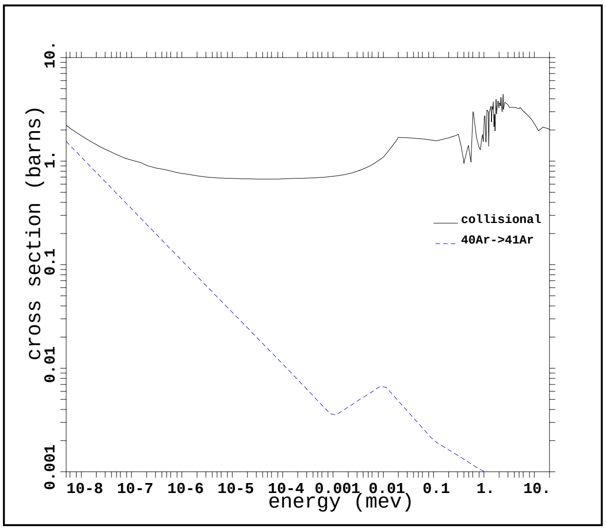


Figure 22. Argon cross-sections. The total cross-section for collisions is almost independent of the neutron energy. For the (n, γ) reaction the cross-section falls like 1/velocity.

of activated $^{41}Ar$ atoms has been calculated by the MCNP code. The concentration of argon in the air is 1.3% by weight. The spectrum of the neutrons and the flux distribution inside the hall have been calculated with 700 ppm of B in the concrete. The B doping of the walls (including the roof and the floor) not only helps to shield the outgoing radiation but also strongly lowers the thermal neutron flux inside the hall. Consequently the number of activated $^{41}Ar$ atoms comes out to be 15 times lower than without any B.

The number of activated $^{41}Ar$ atoms produced by 500 pulses during one year is $2.22 \cdot 10^{14}$ atoms/year. Together with the half life period of 1.83 hours this leads to the annual averaged activity of $2.34 \cdot 10^{10}$ Bq. Under the assumption that the total air volume in the hall of $2.4 \cdot 10^4$ m$^3$ is exchanged every hour by a forced ventilation the exhausted air will be contaminated by the averaged concentration of 110 Bq/m$^3$ due to this $^{41}Ar$ activity. As this level is below the legal limit of 200 Bq/m$^3$ there is no need for any special permission.

Of very little importance is the production of the ß emitting radionuclide $^{14}C$ by the $^{14}N(n,p)^{14}C$ reaction. This very long living isotope ($T_{1/2}$ = 5 730 years) contaminates the exhausted air by the time averaged activity concentration of only $1.7 \cdot 10^{-3}$ Bq/m$^3$. This is completely negligible compared to the legally allowed 8 000 Bq/m$^3$.

# Radioactivity in the Environment

## Dispersion af Argon

In order to assess the dose delivered by the activated air to exposed populations simple calculations were performed based on environmental transport and dosimetric models as described in „Allgemeine Verwaltungsvorschrift zu §45 Strahlenschutzverordnung: Ermittlung der Strahlenexposition durch die Ableitung radioaktiver Stoffe aus kerntechnischen Anlagen oder Einrichtungen“ of 21 February 1990[23]. In particular the long-term propagation factors describing prolonged releases of activity concentrations averaged over weather conditions and depending on the height above ground are used in the calculations. For β-submersion a value of $7 \cdot 10^{-5}$ s/m$^3$ and for γ-submersion $2 \cdot 10^{-3}$ s/m$^2$ were taken from diagrams given in annex 8 and 10 of the reference mentioned. In the case of the most relevant $^{41}Ar$ exaust activity of $2.34 \cdot 10^{10}$ Bq/year the exposure due to β- and γ-submersion yields a total annual dose of about 0.06 µSv, where dose factors of $2.7 \cdot 10^{-14}$ (Sv/s)/(Bq/m$^3$) for β-submersion and $4.3 \cdot 10^{-16}$ (Sv/s)/(Bq/m$^2$) for γ-submersion were used.

## Emission and Dispersion of Tritium

Tritium is the result of the (d,p) reaction path which has the same proability as the neutron production path (d,n). Therefore, every experimental pulse produces as many tritium atoms ($T_{1/2}$ = 12.3 y) as neutrons. Under the assumption that all the tritium will be pumped from the torus and exhausted together with the air from the hall leads to the time averaged activity of 260 Bq/m$^3$. This activity of the exhaust is more than a factor 10 below the legally tolerated level of 3 000 Bq/m$^3$.

The effect of tritium inhaled by exposed people in the vicinity of the plant has been estimated using the long-term propagation factor as given above, the breathing rate $2.32 \cdot 10^{-4}$ m$^3$/s, and the dose-factor for inhalation $1.6 \cdot 10^{-11}$ Sv/Bq. The annual averaged tritium exaust activity of $5.4 \cdot 10^{10}$ Bq corresponding to $3 \cdot 10^{19}$ tritons/year yields a maximum annual dose of

[23] Bundesanzeiger, Jahrgang 42, Nummer 64a, 1990

only about 0.014 μSv. Tritium therefore contributes with about a quarter only to the total dose rate due to the exhaust of the activated air. Consequently the total dose, which was obtained with very conservative assumptions, is orders of magnitudes below legally tolerated values.

# Heat Load to the Coils

The superconductor compound of the coils is the most sensitive component for any heat deposition. Its temperature increase has to stay within very low limits not to destroy the superconductivity. One experimental pulse of 10 s duration produces $6 \cdot 10^{16}$ neutrons of 2.5 MeV. This represents an energy of $1.5 \cdot 10^{17}$ MeV or 24.0 kJ. MCNP calculations have been done to evaluate the energy deposited by the neutrons. The first result is that 14.6 kJ, which is 62% of the total energy, are deposited in the concrete walls surrounding the experiment (floor, ceiling, and wall). The rest of 9.4 kJ gets into the structure of the experiment.

## Energy Deposition of Neutrons

The geometry of the coils has been described before. The details and the material compositions are given in the appendix at Table A-I and the MCNP input file. The mf coils are most sensitive to any temperature increase because the B field is highest at their superconductor windings. The af coils, on the other hand, experience a lower B field and in addition to this a lower energy deposition because of the lower neutron flux. For one pulse Fig. 23 shows the energy deposition to all mf coils and to all af coils (the latter multiplied by 10 for scaling purposes).

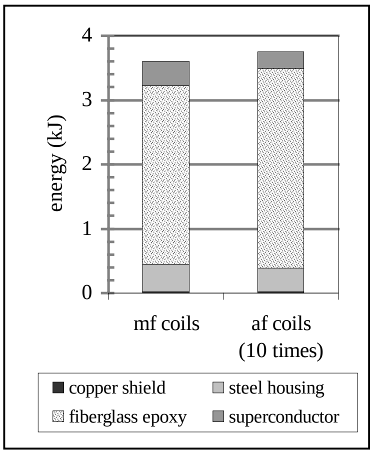


Figure 23. Most of the energy is deposed to the fiberglass epoxy. The energy deposition to the af coils is 10 times less than to the mf coils.

Splitting up the energy at the mf coils to the various materials shows the following:

- By far most of the energy, 2.78 kJ, is deposed to the fiberglass epoxy. This is due to the many light elements contained in the fiberglass epoxy.
- The steel of the coil housings and the superconductor itself get only the comparitively low energies of 0.43 kJ and 0.37 kJ.
- Taking all this together, including even the energy of 0.016 kJ which is deposed to the copper shields, the total energy of 3.60 kJ has to be taken away by the liquid helium cooling system. This is well within the capacity of the projected cooling system.

The total energy deposition to the af coils is close to 10% of the one to the mf coils. But the masses of the af coils are only 17% of that of the mf coils. Therefore the specific heat load kJ/g to the af coils is 60% of that to the mf coils.

## Absorption of Photons

The photon radiation of the activated isotopes is mostly absorbed within the structure materials. The photon energy typically ranges from 0.5 MeV to 1 MeV. Within the superconducting coils Al, Nb, and Cu are the isotopes with the largest activity. The dominant activity comes from $^{28}Al$ up to 4 minutes after the pulse and afterwards $^{94}Nb$ and $^{66}Cu$ contribute about equal amounts to the activity. Taking as an upper limit that 0.5 MeV of each emitting photon gets absorbed within the superconductor (3 cm of iron attenuate a flux of 1 MeV photons by a factor 2) the deposition of power by the absorption of photons can be estimated. At Fig. 24 is shown the temporal decay of the deposed

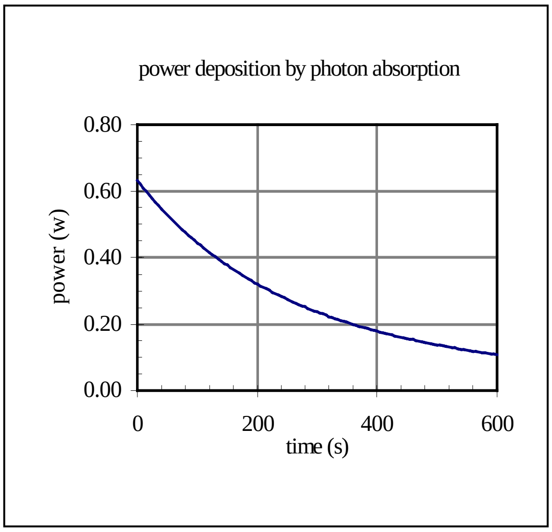


Figure 24. The absorption of the photon flux leads to an initial power deposition of 0.63 W on the sum of all mf coils.

power for the sum of all mf coils. Starting with 0.63 W immediately after the pulse the power decreases almost exponentially to 0.11 W after 5 min. The time integrated power, which is the energy deposed up to this time, is 167 J. This is far below the energy deposed by the neutrons of one pulse and can therefore be neglected for any cooling considerations.

The photon power absorbed in the af coils is as low as 7.5% of that in the mf coils. By the same argument as before that the masses of the af coils are only 17% of that of the mf coils the specific power load W/g at the af coils is 44% of that at the mf coils.

# Conclusions

The neutron transport and the activation of various materials have been calculated for a very detailed but still approximated geometry model of the W 7-X experiment. It has been shown that the neutron flux from the high performance plasma can be sufficiently shielded to the outside by concrete walls. The radiation of the activated steel structure decays to tolerable values within less than ten years after the lifetime of the experiment. The radioactivity in the environment stays below any safety hazard level.

Further studies will be needed to evaluate the biological dose equivalent rate by the decaying radiation near the experiment and in particular inside the torus. This will be important because maintenance and repair demand access to the experiment. No remote handling is forseen for the W 7-X.

The nonuniformities of the neutron yield to the first wall and of the activation of components near to the plasma demand a more realistic three dimensional geometry model for the transport calculations. This is possible to be set up for the MCNP code but turns out to be fairly complicated.

The impact of the neutrons on various diagnostic equipments could be evaluated by using the geometry model as outlined in this report.

# Appendix

The details of the geometry and the positions and dimensions of all individual machine components are listed in Table A-I. The numbers shown describe one mf coil and one af coil only. The full series of coils is generated by rotating the mf coil by multiples of 7.2° and the af coil by multiples of 18° around the central axis in $\phi$–direction. The torus is represented by a straight cylinder with the given dimensions for the angular range of 3.6° only and rotating this cylinder by multiples of 3.6° around the central axis in $\phi$–direction. The cryostat, the ring support, the x-elements, the ports, the control coils, and the divertors are set up by the MCNP code in a very similar manner.

The volume and masses given at Table A-I are calculated from the geometrical dimensions. Most of these volumes and consequently of the masses cannot be simply calculated by the MCNP code. Nevertheless by running the MCNP code with an appropriate neutron source on a sphere surronding the whole experiment and evaluating the flux in the void cells, i.e. taking all the materials out, the fluxes in the cells are proportional to their volumes. These calculations, within their statistical accuracy, coincide with the real geometrical volumes.

The masses used for the MCNP code differ slightly (by 10% at most) from the masses taken from the real design. This results from the concept of taking correctly the overall dimensions of the experiment and at the same time taking correctly the wall thicknesses of the torus and the cryostat in order not to disturb their shielding quality.

The chemical composition of the various materials used are listed at Table A-II. From the relative weight fraction of each chemical constituent and their abundance together with the material density and Avogadro‘s number the atom densities have been calculated. For the MCNP code this atom density has to be expressed in units of atoms/(barn·cm) by the formula: 0.6023 · density(g/cm$^3$) / atomic mass number · relative weight fraction · abundance.

The total input for the MCNP code is shown at the input file. The particular version listed here has been used for calculating the activation of the various materials. The „data cards presently not in use“ at the end of the input file by having inserting those appropriately had been used for calculating the fluxes and dose rates.

**Table A-I.**

## Dimensions,Volumes, and Masses of all Components

| **50 mf coils** | | | | | one mf-coil | | all 50 mf-coils | |
|---|---|---|---|---|---|---|---|---|
| | distance from plasma (cm) | | | dnsity g/cm^3 | volume cm^3 | mass g | volume cm^3 | mass g |
| inside | | 123.85 | superconductor | 4.064 | 2.67E+05 | 1.09E+06 | 1.34E+07 | 5.43E+07 |
| plus copper heat shield | 0.15 | 124.00 | fiberglass epoxy | 2.760 | 1.29E+05 | 3.56E+05 | 6.45E+06 | 1.78E+07 |
| plus steel housing | 3.00 | 127.00 | steel 1.4429 | 7.876 | 2.80E+05 | 2.20E+06 | 1.40E+07 | 1.10E+08 |
| plus fiberglass epoxy | 1.90 | 128.90 | copper heat shield | 8.933 | 1.47E+04 | 1.31E+05 | 7.35E+05 | 6.57E+06 |
| plus superconductor | 19.20 | 148.10 | | sum = | 6.91E+05 | 3.78E+06 | 3.45E+07 | 1.89E+08 |
| plus fiberglass epoxy | 1.90 | 150.00 | | | | | | |
| plus steel housing | 4.00 | 154.00 | | | | | | |
| plus copper heat shield | 0.15 | 154.15 | | | | | | |
| | distance from coil midplane (cm) | | | | | | | |
| left surface | | -13.05 | | | | | | |
| plus copper heat shield | 0.15 | -12.90 | | | | | | |
| plus steel housing | 3.00 | -9.90 | | | | | | |
| plus fiberglass epoxy | 1.90 | -8.00 | | | | | | |
| plus superconductor | 16.00 | 8.00 | | | | | | |
| plus fiberglass epoxy | 1.90 | 9.90 | | | | | | |
| plus steel housing | 3.00 | 12.90 | | | | | | |
| plus copper heat shield | 0.15 | 13.05 | | | | | | |

| **20 af coils** | | | | | one af-coil | | all 20 af coils | |
|---|---|---|---|---|---|---|---|---|
| | distance from plasma (cm) | | | dnsity g/cm^3 | volume cm^3 | mass g | volume cm^3 | mass g |
| inside | | 156.45 | superconductor | 4.064 | 7.33E+04 | 2.98E+05 | 1.47E+06 | 5.96E+06 |
| plus copper heat shield | 0.15 | 156.60 | fiberglass epoxy | 2.760 | 6.99E+04 | 1.93E+05 | 1.40E+06 | 3.86E+06 |
| plus steel housing | 2.00 | 158.60 | steel 1.4429 | 7.876 | 1.32E+05 | 1.04E+06 | 2.65E+06 | 2.09E+07 |
| plus fiberglass epoxy | 1.40 | 160.00 | copper heat shield | 8.933 | 1.02E+04 | 9.14E+04 | 2.05E+05 | 1.83E+06 |
| plus superconductor | 7.00 | 167.00 | | sum = | 2.86E+05 | 1.63E+06 | 5.72E+06 | 3.25E+07 |
| plus fiberglass epoxy | 2.30 | 169.30 | | | | | | |
| plus steel housing | 3.00 | 172.30 | | | | | | |
| plus copper heat shield | 0.15 | 172.45 | | | | | | |
| | distance from coil midplane (cm) | | | | | | | |
| left surface | | -8.65 | | | | | | |
| plus copper heat shield | 0.15 | -8.50 | | | | | | |
| plus steel housing | 2.00 | -6.50 | | | | | all coils (50 mf + 20 af) | |
| plus fiberglass epoxy | 1.40 | -5.10 | | | | | volume cm^3 | mass g |
| plus superconductor | 10.20 | 5.10 | | | | superconductor | 1.48E+07 | 6.03E+07 |
| plus fiberglass epoxy | 1.40 | 6.50 | | | | fiberglass epoxy | 7.85E+06 | 2.17E+07 |
| plus steel housing | 2.00 | 8.50 | | | | steel 1.4429 | 1.66E+07 | 1.31E+08 |
| plus copper heat shield | 0.15 | 8.65 | | | | copper | 9.40E+05 | 8.39E+06 |

| **torus** | distance from plasma (cm) | | | dnsity g/cm^3 | coverage of surface | area of ports cm^2 | volume cm^3 | mass g |
|---|---|---|---|---|---|---|---|---|
| inside | | 93.30 | graphite | 2.230 | 100.00% | 2.04E+05 | 1.83E+06 | 4.09E+06 |
| plus graphite tiles | 1.00 | 94.30 | copper plates | 8.933 | 100.00% | | 1.30E+06 | 1.16E+07 |
| plus copper plates | 0.70 | 95.00 | steel 1.4311 | 7.876 | 100.00% | | 7.61E+06 | 5.99E+07 |
| plus torus steel wall | 4.00 | 99.00 | copper heat shield | 8.933 | 100.00% | | 1.95E+05 | 1.74E+06 |
| plus copper heat shield | 0.10 | 99.10 | | | | sum = | 1.09E+07 | 7.73E+07 |

| **cryostat** | distance from plasma (cm) | | | dnsity g/cm^3 | | area of ports cm^2 | volume cm^3 | mass g |
|---|---|---|---|---|---|---|---|---|
| inside | | 211.03 | copper heat shield | 8.933 | | 2.04E+05 | 4.38E+05 | 3.91E+06 |
| plus copper heat shield | 0.10 | 211.13 | steel 1.4311 | 7.876 | | | 1.21E+07 | 9.55E+07 |
| plus torus steel wall | 2.75 | 213.88 | | | | sum = | 1.26E+07 | 9.94E+07 |

| **2 ring supports** | | | | | one ring | | all 2 rings | |
|---|---|---|---|---|---|---|---|---|
| | dimensions (cm) | | | dnsity g/cm^3 | volume cm^3 | mass g | volume cm^3 | mass g |
| big radii (from - to) | 349.00 | 377.00 | steel 1.4429 | 7.876 | 2.87E+06 | 2.26E+07 | 5.75E+06 | 4.53E+07 |
| heights (from - to) | 15.00 | 60.00 | | | | | | |
| **50 x-elements** | | | | | one element | | all 50 elements | |
| | dimensions (cm) | | | dnsity g/cm^3 | volume cm^3 | mass g | volume cm^3 | mass g |
| small radii (from - to) | 124.00 | 154.00 | steel 1.4429 | 7.876 | 2.02E+05 | 1.59E+06 | 1.01E+07 | 7.95E+07 |
| big limiting radius | | 460.00 | | | | | | |
| gap (=coil width) | | 26.10 | | | | | all supports (2 rings + 50 x-elements) | |
| length of circular arc | | 240.89 | | | | | volume cm^3 | mass g |
| | | | | | | steel 1.4429 | 1.58E+07 | 1.25E+08 |

**Table A-I. (contd.)**

## Dimensions,Volumes, and Masses of all Components

| | | | | | | | | |
|---|---|---|---|---|---|---|---|---|
| **30 ports type I** | | | | | one port type I | | all 30 ports type I | |
| | radius of aperture (cm) | | | dnsity g/cm^3 | volume cm^3 | mass g | volume cm^3 | mass g |
| inside | | 27.00 | steel 1.4311 | 7.876 | 2.73E+04 | 2.15E+05 | 8.19E+05 | 6.45E+06 |
| plus steel wall | 1.00 | 28.00 | copper heat shield | 8.933 | 3.80E+03 | 2.99E+04 | 1.14E+05 | 8.97E+05 |
| plus copper heat shield | 0.15 | 28.15 | | sum = | 3.11E+04 | 2.45E+05 | 9.32E+05 | 7.34E+06 |
| | distance from plasma (cm) | | area (cm^2) | | | | | |
| start of port | | 89.50 | 7.47E+04 | | | | | |
| plus length of tube | 143.50 | 233.00 | | | | | | |
| plus thickness of lid | 1.00 | 234.00 | | | | | | |
| **60 ports type II** | | | | | one port type II | | all 60 ports type II | |
| | radius (cm) | | | dnsity g/cm^3 | volume cm^3 | mass g | volume cm^3 | mass g |
| inside | | 25.00 | steel 1.4311 | 7.876 | 2.51E+04 | 1.98E+05 | 1.51E+06 | 1.19E+07 |
| plus steel wall | 1.00 | 26.00 | copper heat shield | 8.933 | 3.53E+03 | 2.78E+04 | 2.12E+05 | 1.67E+06 |
| plus copper heat shield | 0.15 | 26.15 | | sum = | 2.87E+04 | 2.26E+05 | 1.72E+06 | 1.35E+07 |
| | distance from plasma (cm) | | area (cm^2) | | | | all ports (30 type I + 60 type II) | |
| start of port | | 89.50 | 1.29E+05 | | | | volume (cm^3) | mass (g) |
| plus length of tube | 143.50 | 233.00 | | | | steel 1.4311 | 2.33E+06 | 1.83E+07 |
| plus thickness of lid | 1.00 | 234.00 | | | | copper | 3.26E+05 | 2.56E+06 |
| | | | | | | area (cm^2) = | 2.04E+05 | |

| | | | | | | | | |
|---|---|---|---|---|---|---|---|---|
| **10 control coils** | | | | | one control coil | | all 10 control coils | |
| | distance from plasma (cm) | | | dnsity g/cm^3 | volume cm^3 | mass g | volume cm^3 | mass g |
| inside radius | | 86.00 | steel 1.4311 | 7.876 | 1.68E+03 | 1.32E+04 | 1.68E+04 | 1.32E+05 |
| plus steel housing | 0.30 | 86.30 | copper windings | 8.933 | 4.71E+03 | 4.20E+04 | 4.71E+04 | 4.20E+05 |
| plus copper windings | 3.62 | 89.92 | | sum = | 6.38E+03 | 5.53E+04 | 6.38E+04 | 5.53E+05 |
| plus steel housing | 0.30 | 90.22 | | | | | | |
| | distance (cm) from poloidal plane through mid of coil | | mean radius | 88.11 | | | | |
| toroidal start y | | -70.00 | | | | | | |
| plus steel housing | 0.30 | -69.70 | | | | | | |
| plus copper windings | 3.62 | -66.08 | | | | | | |
| plus steel housing | 0.30 | -65.78 | | | | | | |
| plus gap | 131.56 | 65.78 | | | | | | |
| plus steel housing | 0.30 | 66.08 | | | | | | |
| plus copper windings | 3.62 | 69.70 | | | | | | |
| plus steel housing | 0.30 | 70.00 | | | | | | |
| | distance (cm) from tangential plane at R = 550 cm | | | | | | | |
| poloidal start x | | -22.00 | | | | | | |
| plus steel housing | 0.30 | -21.70 | | | | | | |
| plus copper windings | 3.62 | -18.08 | | | | | | |
| plus steel housing | 0.30 | -17.78 | | | | | | |
| plus gap | 35.56 | 17.78 | | | | | | |
| plus steel housing | 0.30 | 18.08 | | | | | | |
| plus copper windings | 3.62 | 21.70 | | | | | | |
| plus steel housing | 0.30 | 22.00 | | | | | | |

| | | | | | | | | |
|---|---|---|---|---|---|---|---|---|
| **10 divertors** | | | | | | one divertor | | all 10 divertors |
| | distance from plasma (cm) | | | dnsity g/cm^3 | area cm^2 | volume cm^3 | mass g | mass g |
| inside radius | | 80.035 | vacuum | 0.000 | 3.30E+04 | | | |
| plus graphite tiles | 1.300 | 81.335 | graphite | 1.900 | 3.30E+04 | 4.29E+04 | 8.15E+04 | 8.15E+05 |
| plus mo tzm | 0.750 | 82.085 | tzm | 10.200 | 3.29E+04 | 2.47E+04 | 2.52E+05 | 2.52E+06 |
| plus solder | 0.015 | 82.100 | solder | 10.500 | 3.29E+04 | 4.94E+02 | 5.18E+03 | 5.18E+04 |
| plus copper support | 0.900 | 83.000 | copper | 8.933 | 3.29E+04 | 2.96E+04 | 2.64E+05 | 2.64E+06 |
| plus water | 1.000 | 84.000 | water | 0.998 | 3.28E+04 | 3.28E+04 | 3.28E+04 | 3.28E+05 |
| | distance (cm) from poloidal plane through mid of divertor | | | | | | sum = | 6.36E+06 |
| toroidal start | | -45.00 | | | | | | |
| plus wisth | 90.00 | 45.00 | | | | | | |
| | distance (°) from poloidal plane through mid of coil | | | | | | | |
| poloidal start | | 0° | | | | | | |
| plus length | 36° | 36° | | | | | | |

**Table A-II**

**Material Compositions and Atom Densities**

| **SS 1.4429** | | | | density g/cm^3 | **7.876** |
|---|---|---|---|---|---|
| | weight contribution | isotop | mass number | abundance | atoms/(b*cm) |
| Cr | 17.50% | $^{50}$Cr | 50 | 4.345% | 7.21E-04 |
| Mn | 2.00% | $^{55}$Mn | 55 | 100% | 1.72E-03 |
| Fe | 64.73% | $^{54}$Fe | 54 | 5.80% | 3.30E-03 |
| Co | 0.005% | $^{59}$Co | 59 | 100% | 4.02E-06 |
| Ni | 13.00% | $^{58}$Ni | 58 | 68.08% | 7.24E-03 |
| Mo | 2.75% | $^{92}$Mo | 92 | 14.84% | 2.10E-04 |
| Mo | 2.75% | $^{98}$Mo | 98 | 24.13% | 3.21E-04 |
| Mo | 2.75% | $^{100}$Mo | 100 | 9.63% | 1.26E-04 |
| V | 0.02% | $^{51}$V | 51 | 99.75% | 1.86E-05 |
| **SS 1.4311** | | | | density g/cm^3 | **7.876** |
| | weight contribution | isotop | mass number | abundance | atoms/(b*cm) |
| Cr | 18.00% | $^{50}$Cr | 50 | 4.35% | 7.42E-04 |
| Mn | 2.00% | $^{55}$Mn | 55 | 100% | 1.72E-03 |
| Fe | 69.98% | $^{54}$Fe | 54 | 5.80% | 3.57E-03 |
| Co | 0.005% | $^{59}$Co | 59 | 100% | 4.02E-06 |
| Ni | 10.00% | $^{58}$Ni | 58 | 68.08% | 5.57E-03 |
| V | 0.02% | $^{51}$V | 51 | 99.75% | 1.86E-05 |
| **copper** | | | | density g/cm^3 | **8.933** |
| | weight contribution | isotop | mass number | abundance | atoms/(b*cm) |
| Cu | 100% | $^{63}$Cu | 63 | 69.17% | 5.91E-02 |
| Cu | 100% | $^{65}$Cu | 65 | 30.83% | 2.55E-02 |
| **superconductor** | | | | density g/cm^3 | **4.064** |
| | weight contribution | isotop | mass number | abundance | atoms/(b*cm) |
| Mg | 0.710% | $^{26}$Mg | 26 | 11.01% | 7.36E-05 |
| Al | 46.20% | $^{27}$Al | 27 | 100% | 4.19E-02 |
| Si | 0.40% | $^{30}$Si | 30 | 3.10% | 1.01E-05 |
| Ti | 3.93% | $^{50}$Ti | 50 | 5.40% | 1.04E-04 |
| Cr | 0.178% | $^{50}$Cr | 50 | 4.35% | 3.79E-06 |
| Fe | 0.195% | $^{54}$Fe | 54 | 5.80% | 5.13E-06 |
| Cu | 37.50% | $^{63}$Cu | 63 | 69.17% | 1.01E-02 |
| Cu | 37.50% | $^{65}$Cu | 65 | 30.83% | 4.35E-03 |
| Nb | 10.77% | $^{93}$Nb | 93 | 100% | 2.83E-03 |
| **solder** | | | | density g/cm^3 | **10.5** |
| | weight contribution | isotop | mass number | abundance | atoms/(b*cm) |
| Ti | 5.00% | $^{50}$Ti | 50 | 5.40% | 3.42E-04 |
| Cu | 20.00% | $^{63}$Cu | 63 | 69.17% | 1.39E-02 |
| Cu | 20.00% | $^{65}$Cu | 65 | 30.83% | 6.00E-03 |
| Ag | 75.00% | $^{107}$Ag | 107 | 51.84% | 2.30E-02 |
| Ag | 75.00% | $^{109}$Ag | 109 | 48.16% | 2.10E-02 |
| **tzm** | | | | density g/cm^3 | **10.5** |
| | weight contribution | isotop | mass number | abundance | atoms/(b*cm) |
| Mo | 100% | $^{92}$Mo | 92 | 14.84% | 1.02E-02 |
| Mo | 100% | $^{98}$Mo | 98 | 24.13% | 1.56E-02 |
| Mo | 100% | $^{100}$Mo | 100 | 9.63% | 6.09E-03 |
| **air** | | | | density g/cm^3 | **0.0013** |
| | weight contribution | isotop | mass number | abundance | atoms/(b*cm) |
| Ar | 1.30% | $^{40}$Ar | 40 | 99.60% | 2.53E-07 |

## Input File for MCNP 4B

```
w7-x - 6.0e16 neutrons at 2.5 mev - cyl.hall: r=17.7 m, h=24.0 m, vol=2.4e4 m3
c
c ########################################################################################
c
c |_____cell cards______|
c
c ----- ----- outermost cell for testing the geometry only ----- -----
 1001  0          9999                                      imp:n=0  $ outside world
 1000  0         (1000:-1001 :1002)-9999                    imp:n=1  $ additional cell
c
c ----- ----- real start of cell cards ----- -----
c 1000  0          1000:-1001:1002                           imp:n=0  $ outside world
  10   0         -1000  1001 -1002 (950:-951:952)           imp:n=1  $ outside of concrete shield
c ----- ----- from inside surface to outside surface of concrete shield ----- -----
  11 19 -2.2505  -907  951 -908                             imp:n=2  $ floor
  12 19 -2.2505  -907  909 -952                             imp:n=2  $ ceiling
  13 19 -2.2505   907 -950  951  -952                       imp:n=2  $ wall
  50  2 -1.30e-3 -907  908 -909 ( 904:-905: 906)            imp:n=1  $ from mid of hall to wall
  51  2 -1.30e-3 -904  905 -906 (-900: 901:-902:903)        imp:n=1  $ from machine to mid of hall
c ----- ----- full toroidal machine enclosed between two cylinders ----- -----
  70   0          900 -901 902 -903          fill=1         imp:n=1  $ full toroidal machine
c ----- ----- all five moduls ----- -----
  80   0         #81 #82 #83 #84 #85                  u=1    imp:n=1  $ empty
c
  81   0          9 -10                      fill=2   u=1    imp:n=1  $ 1.full modul -36 < phi < +36
  82  like 81 but                    trcl=1                           $ 2.full module
  83  like 81 but                    trcl=2                           $ 3.full module
  84  like 81 but                    trcl=3                           $ 4.full module
  85  like 81 but                    trcl=4                           $ 5.full module
c ----- ----- one full modul ----- -----
  86   0         #87 #88                              u=2    imp:n=1  $ empty
c
  87   0          1                          fill=10  u=2    imp:n=1  $ 1/2 modul at phi > 0
  88  like 87 but                    trcl=5                           $ rotated by 180
c ----- ----- segments for 1/2 modul ----- -----
  91   0            -2                       fill=100 u=10   imp:n=1  $ 1.segment:       phi < 7.2
  92   0          2 -3                       fill=200 u=10   imp:n=1  $ 2.segment: 7.2 < phi < 14.4
  93   0          3 -4                       fill=300 u=10   imp:n=1  $ 3.segment:14.4 < phi < 21.6
  94   0          4 -5                       fill=400 u=10   imp:n=1  $ 4.segment:21.6 < phi < 28.8
  95   0          5                          fill=500 u=10   imp:n=1  $ 5.segment:28.8 < phi
c
c ----- ----- cells for 1.segment ----- ----- cells for 1.segment ----- -----
c ----- ----- ports ----- -----
 100   0        #101 #106 #111               fill=110 u=100  imp:n=1  $ empty
c
 101   0             -102  105 -107          fill=111 u=100  imp:n=1  $ type I phi=0,theta=0
 102   0             -100 -106                        u=111  imp:n=5  $ inside of port
 103 11 -7.876   100 -101 -106: 106                   u=111  imp:n=10 $ steel wall
 104 14 -8.933   101      -106                        u=111  imp:n=10 $ copper heat shield
c
 106   0             -112  115 -117          fill=112 u=100  imp:n=1  $ type II phi=0,theta=45
 107   0             -110 -116                        u=112  imp:n=5  $ inside of port
 108 11 -7.876   110 -111 -116: 116                   u=112  imp:n=10 $ steel wall
 109 14 -8.933   111      -116                        u=112  imp:n=10 $ copper heat shield
c
 111   0             -122  125 -127          fill=113 u=100  imp:n=1  $ type II phi=0,theta=-45
 112   0             -120 -126                        u=113  imp:n=5  $ inside of port
 113 11 -7.876   120 -121 -126: 126                   u=113  imp:n=10 $ steel wall
 114 14 -8.933   121      -126                        u=113  imp:n=10 $ copper heat shield
c ----- ----- coils ----- -----
 150  0         #151                         fill=120 u=110  imp:n=1  $ empty
c
 151  0          201 -208  211 -218          fill=121 u=110  imp:n=1  $ 1.modular coil
 152 14 -8.933  -202: 207:-212: 217                   u=121  imp:n=1  $ copper heat shield
 153 10 -7.876 (-203: 206:-213: 216)202 -207 212 -217 u=121  imp:n=1  $ steel housing
 154 12 -2.76  (-204: 205:-214: 215)203 -206 213 -216 u=121  imp:n=2  $ fiberglass epoxy
 155 13 -4.064   204 -205  214 -215                   u=121  imp:n=2  $ superconductor windings
c ----- ----- support structure ----- -----
 157  0         #158 #159                    fill=130 u=120  imp:n=1  $ empty
c
 158 10 -7.876   240 -241 (242  -243:244 -245)        u=120  imp:n=100 $ ring supports
 159 10 -7.876   246 -247 -248 (-210:219)             u=120  imp:n=10  $ x-elements
c ----- ----- toroidal components ----- -----
 160  0         #161 #162                    fill=140 u=130  imp:n=1  $ empty
c
 161  1 -1e-10       -500                             u=130  imp:n=2  $ plasma
 162  0          510                         fill=141 u=130  imp:n=1  $ from inside wall of torus
 163 15 -2.230       -511                             u=141  imp:n=1  $ graphite tiles
 164 14 -8.933   511 -512                             u=141  imp:n=1  $ copper plates
```

```
 165 11 -7.876   512 -513                             u=141  imp:n=1  $ torus steel wall
 166 14 -8.933   513 -514                             u=141  imp:n=1  $ copper heat shield
 167  0          514 -520                             u=141  imp:n=.2 $ from shield to shield
 168 14 -8.933   520 -521                             u=141  imp:n=1  $ copper heat shield
 169 11 -7.876   521 -522                             u=141  imp:n=1  $ cryostat wall
 170  2 -1.30e-3 522                                  u=141  imp:n=1  $ outside of cryostat
c ----- ----- structures inside torus ----- -----
 171  0          #180                                 u=140  imp:n=1  $ empty
c
 180  0          334 -339 330 332 -333 340   fill=145 u=140  imp:n=1  $ divertor
 181 15 -2.230       -335                             u=145  imp:n=2  $ graphite tiles
 182 16 -10.20   335 -336                             u=145  imp:n=2  $ tzm molybdenum
 183 17 -10.50   336 -337                             u=145  imp:n=2  $ solder
 184 14 -8.933   337 -338                             u=145  imp:n=2  $ copper support plates
 185 18 -0.998   338                                  u=145  imp:n=2  $ cooling water
c
c ----- ----- cells for 2.segment ----- ----- cells for 2.segment ----- -----
c ----- ----- ports ----- -----
 200  0         #201 #202 #203              fill=210 u=200  imp:n=1  $ empty
 201 like 101                   but trcl=8           u=200           $ type I phi=14.4,theta=0
 202 like 106                   but trcl=8           u=200           $ type II phi=14.4,theta=45
 203 like 111                   but trcl=8           u=200           $ type II phi=14.4,theta=-45
c ----- ----- coils ----- -----
 250  0         #251 #252                   fill=220 u=210  imp:n=1  $ empty
 251 like 151                   but trcl=7           u=210           $ 2.modular coil at phi=10.8
 252  0         221 -228  231 -238          fill=221 u=210  imp:n=1  $ 1.auxiliary coil at phi=9
 253 14 -8.933  -222: 227:-232: 237                  u=221  imp:n=5  $ copper heat shield
 254 10 -7.876 (-223: 226:-233: 236)222 -227 232 -237 u=221  imp:n=5  $ steel housing
 255 12 -2.76  (-224: 225:-234: 235)223 -226 233 -236 u=221  imp:n=5  $ fiberglass epoxy
 256 13 -4.064   224 -225  234 -235                  u=221  imp:n=10 $ superconductor windings
c ----- ----- support structure ----- -----
 257  0         #258 #259                   fill=230 u=220  imp:n=1  $ empty
 258 like 158                   but trcl=7           u=220  imp:n=5  $ ring supports
 259 like 159                   but trcl=7           u=220  imp:n=2  $ x-elements
c ----- ----- toroidal components ----- -----
 260  0        #261 #262                    fill=240 u=230  imp:n=1  $ empty
 261 like 161                   but trcl=7           u=230           $ plasma
 262 like 162                   but trcl=7           u=230           $ from wall to cryostat
c ----- ----- structures inside torus ----- -----
 263  0        #265 #266                             u=240  imp:n=1   $ empty
 265  0        334 -339 332 -333 340 trcl=7  fill=145 u=240  imp:n=1   $ divertor
 266  0        316 -319 300 -307 308 -315 320
                                    trcl=13 fill=241 u=240  imp:n=1   $ control coil
 267  0          303 -304  311 -312                  u=241  imp:n=50  $ inside of coil
 268 14 -8.933  (309 -310 :313 -314) 317 -318        u=241  imp:n=20  $ copper phi-windings
 269 10 -7.876 (-309 :310 -311 :312 -313 :314)
              :(-317 :318)(309 -310 :313 -314)       u=241  imp:n=20  $ steel phi-housing
 270 14 -8.933  (301 -302 :305 -306) 311 -312   317 -318
                                                     u=241  imp:n=100 $ copper theta-windings
 271 10 -7.876   311 -312((301 -302 :305 -306)(-317 :318)
              :(-301 :302 -303 :304 -305 :306))      u=241  imp:n=100 $ steel theta-housing
c
c ----- ----- cells for 3.segment ----- ----- cells for 3.segment ----- -----
c ----- ----- ports ----- -----
 300   0       #301 #302 #303 #304 #305 #306 fill=310 u=300  imp:n=1  $ empty
 301 like 201                                    but u=300           $ type I from 2.segment
 302 like 202                                    but u=300           $ type II from 2.segment
 303 like 203                                    but u=300           $ type II from 2.segment
 304 like 101                   but trcl=9           u=300           $ type I phi=21.6,theta=0
 305 like 106                   but trcl=9           u=300           $ type II phi=21.6,theta=45
 306 like 111                   but trcl=9           u=300           $ type II phi=21.6,theta=-45
c ----- ----- coils ----- -----
 350  0        #351                         fill=320 u=310  imp:n=1  $ empty
 351 like 151                   but trcl=8           u=310           $ 3.modular coil at phi=14.4
c ----- ----- support structure ----- -----
 357  0        #358 #359                    fill=330 u=320  imp:n=1  $ empty
 358 like 158                   but trcl=8           u=320  imp:n=5  $ ring supports
 359 like 159                   but trcl=8           u=320  imp:n=2  $ x-elements
c ----- ----- toroidal components ----- -----
 360  0        #361 #362                    fill=340 u=330  imp:n=1  $ empty
 361 like 161                   but trcl=8           u=330           $ plasma
 362 like 162                   but trcl=8           u=330           $ from wall to cryostat
c ----- ----- structures inside torus ----- -----
 363  0        #365 #366                             u=340  imp:n=1  $ empty
 365 like 265                   but trcl=8           u=340           $ divertor
 366 like 266                   but trcl=14          u=340           $ control coil
c
c ----- ----- cells for 4.segment ----- ----- cells for 4.segment ----- -----
c ----- ----- ports ----- -----
 400   0       #401 #402 #403               fill=410 u=400  imp:n=1  $ empty
 401 like 304                                    but u=400           $ type I from 3.segment
 402 like 305                                    but u=400           $ type II from 3.segment
```

```
 403 like 306                                   but u=400           $ type II from 3.segment
c ----- ----- coils ----- -----
 450  0        #451 #452                   fill=420 u=410  imp:n=1  $ empty
 451 like 151                    but trcl=9          u=410           $ 4.modular coil at phi=25.2
 452 like 252                    but trcl=26         u=410           $ 2.auxiliary coil at phi=27
c ----- ----- support structure ----- -----
 457  0        #458 #459                   fill=430 u=420  imp:n=1  $ empty
 458 like 158                    but trcl=9          u=420  imp:n=5  $ ring supports
 459 like 159                    but trcl=9          u=420  imp:n=2  $ x-elements
c ----- ----- toroidal components ----- -----
 460  0        #461 #462                   fill=440 u=430  imp:n=1  $ empty
 461 like 161                    but trcl=9          u=430           $ plasma
 462 like 162                    but trcl=9          u=430           $ from wall to cryostat
c ----- ----- structures inside torus ----- -----
 463  0        #465 #466                            u=440  imp:n=1  $ empty
 465 like 265                    but trcl=9          u=440           $ divertor
 466 like 266                    but trcl=15         u=440           $ control coil
c
c ----- ----- cells for 5.segment ----- ----- cells for 5.segment ----- -----
c ----- ----- ports ----- -----
 500   0       #501 #502 #503              fill=510 u=500  imp:n=1  $ empty
 501 like 101                    but trcl=11         u=500           $ type I phi=36,theta=0
 502 like 106                    but trcl=11         u=500           $ type II phi=36,theta=45
 503 like 111                    but trcl=11         u=500           $ type II phi=36,theta=-45
c ----- ----- coils ----- -----
 550  0        #551                        fill=520 u=510  imp:n=1  $ empty
 551 like 151                    but trcl=10         u=510           $ 5.modular coil at phi=32.4
c ----- ----- support structure ----- -----
 557  0        #558 #559                   fill=530 u=520  imp:n=1  $ empty
 558 like 158                    but trcl=10         u=520  imp:n=5  $ ring supports
 559 like 159                    but trcl=10         u=520  imp:n=2  $ x-elements
c ----- ----- toroidal components ----- -----
 560  0        #561 #562                   fill=540 u=530  imp:n=1  $ empty
 561 like 161                    but trcl=10         u=530           $ plasma
 562 like 162                    but trcl=10         u=530           $ from wall to cryostat
c ----- ----- structures inside torus ----- -----
 563  0        #565                                 u=540  imp:n=1  $ empty
 565  0         334 -339 -331 332 -333 340
                                     trcl=10 fill=145 u=540  imp:n=1  $ divertor
c
c #######################################################################################

c #######################################################################################
c
c |____surface cards____|
c
c ----- ----- sphere to separate the outside world ----- -----
 9999    so  3000                        $ all surrounding sphere
c ----- ----- hollow cylinder surrounding the machine ----- -----
 900     cz   300                        $ inner cylinder
 901     cz   800                        $ outer cylinder
 902     pz  -250                        $ bottom plane
 903     pz   250                        $ top plane
c ----- ----- full cylinder halfway between the machine and the concrete wall ----- -----
 904     cz  1285                        $ cylinder
 905     pz  -625                        $ bottom plane
 906     pz   825                        $ top plane
c ----- ----- full cylinder at the inside of the concrete wall ----- -----
 907     cz  1770                        $ cylinder
 908     pz -1000                        $ bottom plane
 909     pz  1400                        $ top plane
c ----- ----- full cylinder at the outside of the concrete wall ----- -----
 950     cz  1950                        $ cylinder
 951     pz -1180                        $ bottom plane
 952     pz  1520                        $ top plane
c ----- ----- cylinder surrounding the whole assmbly ----- -----
1000     cz  1951                        $ cylinder
1001     pz -1181                        $ bottom plane
1002     pz  1521                        $ top plane
c ----- ----- poloidal planes ----- -----
   1      py     1e-9                    $ plane at 0 degrees (slightly shifted)
   2   7 py     0                        $ plane at 7.2 degrees
   3   8 py     0                        $ plane at 14.4 degrees
   4   9 py     0                        $ plane at 21.6 degrees
   5  10 py     0                        $ plane at 28.8 degrees
   9  12 py     1e-9                     $ plane at -36 degrees (slightly shifted)
  10  11 py    -1e-9                     $ plane at 36 degrees (slightly shifted)
c ----- ----- port of type I (theta=0) ----- -----
 100  30 cx   27.00                      $ inside radius
 101  30 cx   28.00                      $ +1.00 cm steel wall
 102  30 cx   28.15                      $ +0.15 cm copper heat shield
 105  30 px   89.5                       $ start of port
```

```
 106  30 px  233                         $ +143.5 cm length of tube
 107  30 px  234                         $ +1.0 cm thickness of lid
c ----- ----- port of type II (theta=45) ----- -----
 110  31 cx   25.00                      $ inside radius
 111  31 cx   26.00                      $ +1.00 cm steel wall
 112  31 cx   26.15                      $ +0.15 cm copper heat shield
 115  31 px   89.5                       $ start of port
 116  31 px  233                         $ +143.5 cm length of tube
 117  31 px  234                         $ +1.0 cm thickness of lid
c ----- ----- port of type II (theta=-45) ----- -----
 120  32 cx   25.00                      $ inside radius
 121  32 cx   26.00                      $ +1.00 cm steel wall
 122  32 cx   26.15                      $ +0.15 cm copper heat shield
 125  32 px   89.5                       $ start of port
 126  32 px  233                         $ +143.5 cm length of tube
 127  32 px  234                         $ +1.0 cm thickness of lid
c ---------- modular coil surfaces ----- -----
 201  6 c/y  550  0  123.85              $ inside radius
 202  6 c/y  550  0  124.00              $ +0.15 cm copper heat shield
 203  6 c/y  550  0  127.00              $ +3.00 cm steel housing
 204  6 c/y  550  0  128.90              $ +1.90 cm fiberglass epoxy
 205  6 c/y  550  0  148.10              $ +19.2 cm superconductor windings
 206  6 c/y  550  0  150.00              $ +1.90 cm fiberglass epoxy
 207  6 c/y  550  0  154.00              $ +4.00 cm steel housing
 208  6 c/y  550  0  154.15              $ +0.15 cm copper heat shield
 210  6 py      -13.0501                 $ left surface - epsilon
 211  6 py      -13.05                   $ left surface
 212  6 py      -12.90                   $ +0.15 cm copper heat shield
 213  6 py       -9.90                   $ +3.00 cm steel housing
 214  6 py       -8.00                   $ +1.90 cm fiberglass epoxy
 215  6 py        8.00                   $ +16.0 cm superconductor windings
 216  6 py        9.90                   $ +1.90 cm fiberglass epoxy
 217  6 py       12.90                   $ +3.00 cm steel housing
 218  6 py       13.05                   $ +0.15 cm copper heat shield
 219  6 py       13.0501                 $ right surface + epsilon
c ----- ----- auxiliary coil surfaces ----- -----
 221 25 c/y  550  0  156.45              $ inside radius
 222 25 c/y  550  0  156.60              $ +0.15 cm copper heat shield
 223 25 c/y  550  0  158.60              $ +2.00 cm steel housing
 224 25 c/y  550  0  160.00              $ +1.40 cm fiberglass epoxy
 225 25 c/y  550  0  167.00              $ +7.00 cm superconductor windings
 226 25 c/y  550  0  169.30              $ +2.30 cm fiberglass epoxy
 227 25 c/y  550  0  172.30              $ +3.00 cm steel housing
 228 25 c/y  550  0  172.45              $ +0.15 cm copper heat shield
 231 25 py       -8.65                   $ left surface
 232 25 py       -8.50                   $ +0.15 cm copper heat shield
 233 25 py       -6.50                   $ +2.00 cm steel housing
 234 25 py       -5.10                   $ +1.40 cm fiberglass epoxy
 235 25 py        5.10                   $ +10.2 cm superconductor windings
 236 25 py        6.50                   $ +1.40 cm fiberglass epoxy
 237 25 py        8.50                   $ +2.00 cm steel housing
 238 25 py        8.65                   $ +0.15 cm copper heat shield
c ----- ----- coil support surfaces ----- -----
 240  6 px   349                         $ ring support distance from center
 241  6 px   377
 242     pz   -60                        $ ring support below midplane
 243     pz   -15
 244     pz    15                        $ ring support above midplane
 245     pz    60
 246  6 c/y  550  0  124                 $ x-elements inside radius
 247  6 c/y  550  0  154                 $ x-elements outside radius
 248     cz   460                        $ x-elements termination
c ----- ----- control coil surfaces ----- -----
 300 30 py  -70.0                        $ start in phi direction
 301 30 py  -69.7                        $ +0.3 cm steel housing
 302 30 py  -66.08                       $ +3.62 cm copper windings
 303 30 py  -65.78                       $ +0.3 cm steel housing
 304 30 py   65.78                       $ +117.56 cm length of coil
 305 30 py   66.08                       $ +0.3 cm steel housing
 306 30 py   69.7                        $ +3.62 cm copper windings
 307 30 py   70.0                        $ +0.3 cm steel housing
 308 30 px  -22.0                        $ start in x direction
 309 30 px  -21.7                        $ +0.3 cm steel housing
 310 30 px  -18.08                       $ +3.62 cm copper windings
 311 30 px  -17.78                       $ +0.3 cm steel housing
 312 30 px   17.78                       $ +35.56 cm width of coil
 313 30 px   18.08                       $ +0.3 cm steel housing
 314 30 px   21.7                        $ +3.62 cm copper windings
 315 30 px   22.0                        $ +0.3 cm steel housing
 316     c/y  550  0  86.0               $ inside surface of coil
 317     c/y  550  0  86.3               $ +0.3 cm steel housing
 318     c/y  550  0  89.92              $ +3.62 cm copper windings
```

```
 319    c/y  550  0  90.22               $ +0.3 cm steel housing
 320    pz     1                         $ horizontal limitation
c ----- ----- divertor surfaces ----- -----
 330 21 py   0                           $ start in phi direction
 331 22 py   0                           $ stop in phi direction
 332 23 px  -45.0                        $ start in -x direction
 333 23 px   45.0                        $ stop in +x direction
 334  6 c/y  550  0  80.035              $ inside surface
 335  6 c/y  550  0  81.335              $ +1.3 cm graphite tiles
 336  6 c/y  550  0  82.085              $ +0.75 cm tzm molybdenum
 337  6 c/y  550  0  82.1                $ +0.015 cm solder
 338  6 c/y  550  0  83.0                $ +0.9 cm support plates
 339  6 c/y  550  0  84.0                $ +2.2 cm water cooling
 340    pz     2                         $ horizontal limitation
c ----- ----- toroidally arranged cylinder surfaces ----- -----
 500  6 c/y  550 0 50.00                 $ cylindrical outside surface of plasma
 510  6 c/y  550 0 93.30                 $ cylindrical inside surface of torus wall
 511  6 c/y  550 0 94.30                 $ +1.00 cm graphite tiles
 512  6 c/y  550 0 95.00                 $ +0.70 cm copper plates
 513  6 c/y  550 0 99.00                 $ +4.00 cm torus steel wall
 514  6 c/y  550 0 99.10                 $ +0.10 cm copper heat shield
 520  6 c/y  550 0 211.03                $ cylindrical inside surface of cryostat
 521  6 c/y  550 0 211.13                $ +0.10 cm copper heat shield
 522  6 c/y  550 0 213.88                $ +2.75 cm cryostat steel wall
c ###########################################################################################

c ###########################################################################################
c
c |_____data cards______|
c
c ----- ----- rotation of full moduls ----- -----
 *tr1     0     0    0  72    18   90  3j  90 90 0  $ around z by 72 degrees
 *tr2     0     0    0 144   -54   90  3j  90 90 0  $ around z by 144 degrees
 *tr3     0     0    0 216  -126   90  3j  90 90 0  $ around z by 216 degrees
 *tr4     0     0    0 288  -198   90  3j  90 90 0  $ around z by 288 degrees
c ----- ----- rotation of 1/2 modul ----- -----
  tr5     0     0    0     1 0 0   0 -1 0   0 0 -1  $ rotate around x by 180 degrees
c ----- ----- rotation of modular coils and internal structures----- -----
 *tr6     0     0    0   3.6  86.4 90  3j  90 90 0  $ around z by 3.6 degrees
 *tr7     0     0    0   7.2  82.8 90  3j  90 90 0  $ around z by 7.2 degrees
 *tr8     0     0    0  14.4  75.6 90  3j  90 90 0  $ around z by 14.4 degrees
 *tr9     0     0    0  21.6  68.4 90  3j  90 90 0  $ around z by 21.6 degrees
 *tr10    0     0    0  28.8  61.2 90  3j  90 90 0  $ around z by 28.8 degrees
 *tr11    0     0    0  36.0  54.0 90  3j  90 90 0  $ around z by 36 degrees
 *tr12    0     0    0 -36   126   90  3j  90 90 0  $ around z by -36 degrees
c ----- ----- shift and rotation of control coil ----- -----
 *tr13 -12.56  65.81 0  10.8  79.2 90  3j  90 90 0  $ shift and around z by 10.8 degrees
 *tr14    0     0    0  18.0  72.0 90  3j  90 90 0  $ shift and around z by 18.0 degrees
 *tr15  28.53 -60.62 0  25.2  64.8 90  3j  90 90 0  $ shift and around z by 25.2 degrees
c ----- ----- shift and rotation of divertor ----- -----
 *tr21    0     0    0   0    90.0 90  3j  90 90 0  $ around z by 0.0 degrees, phi-start
 *tr22    0     0    0   7.2  82.8 90  3j  90 90 0  $ around z by 7.2 degrees, phi-stop
 *tr23  550     0    0   3.6  86.4 90  3j  90 90 0  $ shift and around z by 3.6 degrees, x-limits
c ----- ----- rotation of auxiliary coils ----- -----
 *tr25    0     0    0   9.0  81.0 90  3j  90 90 0  $ around z by 9.0 degrees
 *tr26    0     0    0  18.0  72.0 90  3j  90 90 0  $ around z by 18.0 degrees
c ----- ----- shift and poloidal rotation of ports ----- -----
  tr30  550                                         $ shift only
  tr31  550     0    0   .707  0  .707  0  1  0     $ shift and around y by 45 degrees
  tr32  550     0    0   .70   0 -.707  0  1  0     $ shift and around y by -45 degrees
c ###########################################################################################
c
c ----- ----- materials for transport calculations ----- -----
c
c   nuclide identifier   weight fraction       (colors by sequence of this list)
c ----------------------------------------------------------------------------
c     stainless steel: ss 1.4429   rho=7.876 g/cm3
 m10   24000.50c          -0.175                $ cr-nat
       26000.55c          -0.64745              $ fe-nat
       25055.50c          -0.02                 $ mn-55
       28000.50c          -0.13                 $ ni-nat
       27059.50c          -0.00005              $ co-59
       42000.50c          -0.0275               $ mo-nat
c ----------------------------------------------------------------------------
c     stainless steel: ss 1.4311   rho=7.876 g/cm3
 m11   24000.50c          -0.18                 $ cr-nat
       26000.55c          -0.69995              $ fe-nat
       25055.50c          -0.02                 $ mn-55
       28000.50c          -0.10                 $ ni-nat
       27059.50c          -0.00005              $ co-59
c ----------------------------------------------------------------------------
c     fiberglass epoxy            rho=2.760 g/cm3
```

```
 m12    1001.50c          -0.02960                $ h-1
        6000.50c          -0.30856                $ c-nat
        8016.50c          -0.32806                $ o-16
       11023.50c          -0.05787                $ na-23
       12000.50c          -0.01809                $ mg-nat
       13027.50c          -0.00953                $ al-27
       14000.50c          -0.17110                $ si-nat
       20000.50c          -0.07719                $ ca-nat
c -----------------------------------------------------------------------------
c     superconductor nb-ti         rho=4.064 g/cm3
 m13   12000.50c          -0.00710                $ mg-nat
       13027.50c          -0.46175                $ al-27
       14000.50c          -0.00400                $ si-nat
       22000.50c          -0.03929                $ ti-nat
       24000.50c          -0.00178                $ cr-nat
       26000.55c          -0.00200                $ fe-nat
       29000.50c          -0.37539                $ cu-nat
       40000.50c          -0.00102                $ zr-nat
       41093.50c          -0.10767                $ nb-93
c -----------------------------------------------------------------------------
c     water h2o                    rho=0.998 g/cm3
 m18    1001.50c          -0.111                  $ h-1
        8016.50c          -0.889                  $ o-16
c -----------------------------------------------------------------------------
c     air                          rho=1.30e-3 g/cm3
 m2     7014.50c          -0.755                  $ n-14
        8016.50c          -0.232                  $ o-16
       18000.35c          -0.013                  $ ar-nat
c -----------------------------------------------------------------------------
c     molybdenum tzm               rho=10.20 g/cm3
 m16   42000.50c             1                    $ mo-nat
c -----------------------------------------------------------------------------
c     graphite tiles c             rho=2.230 g/cm3
 m15    6000.50c             1                    $ c-nat
c -----------------------------------------------------------------------------
c     deuterium: 1e14 particles/cm3, i.e. 1e-10 particles/(barn*cm)
 m1     1002.55c             1                    $ d-2
c -----------------------------------------------------------------------------
c     copper cu                    rho=8.933 g/cm3
 m14   29000.50c             1                    $ cu-nat
c -----------------------------------------------------------------------------
c     solder                       rho=10.50 g/cm3
 m17   22000.50c          -0.05                   $ ti-nat
       29000.50c          -0.20                   $ cu-nat
       47000.55c          -0.75                   $ ag-nat
c -----------------------------------------------------------------------------
c     los alamos concrete with 700ppm boron         rho = 2.2505 g/cm3
c     (7e-4 of si-nat is substituted by 7e-4 boron-10)
c     from mcnp manual, Test 1, page 5-12, like ASDEX-Upgrade
 m19    1001.50c          -0.004532               $ h-1
        5010.50c          -0.000700               $ b-10
        8016.50c          -0.512597               $ o-16
       11023.50c          -0.011553               $ na-23
       12000.50c          -0.003866               $ mg-nat0
       13027.50c          -0.035548               $ al-27
       14000.50c          -0.359664               $ si-nat
       19000.50c          -0.014219               $ k-nat
       20000.50c          -0.043546               $ ca-nat
       26000.55c          -0.013775               $ fe-nat
c ########################################################################################
c
c ----- ----- source definition ----- --
c source definition for neutrons originating unformly from circular ring source
  sdef  pos=0 0 0 axs=0 0 1 rad=550      $ degenerated cylindrical volume source
        erg=d2  wgt=6.0e16               $ energy distribution for 1e16 neutrons (d-d)
  sp2  -4 -0.004 -2                      $ d-d fusion neutrons for T=4keV plama
c        erg=d2  wgt=3e14                 $ energy distribution for 1e10 neutrons (d-t)
c  sp2  -4 -0.004 -1                      $ d-t fusion neutrons for T=4keV plama
c
c ########################################################################################
  fq0   f e m      $ cells f are columns, fluxes e (evtl. summed over all energies) are rows
c
c ----- ----- activation tallies ----- ----- activation tallies ----- -----
c sd: every tally will be normalized by dividing itself (or the average) to volume=1
c fm: each tally will be multiplied by the energy dependent cross section of the reaction path
c
  fc14   ----- activation of ss 1.4429, density = 7.876 g/cm3  -----
  f14:n (153 254)                         $ coil_housings
        (158 159 258 259 358 359 458 459 558 559) $ support_rings  x_elements
        (269 271)       t                  $ control_coils  total
  sd14  1.303e8                            $ density * evaluated volumes
                 1.233e8
```

```
       1.326e5     2.537e8
c         atoms/(b*cm)  mat.number  reaction path
  fm14:n   (7.21e-4        208          102)      $ cr-50(n,gamma)cr-51
           (1.72e-3        209          102)      $ mn-55(n,gamma)mn-56
           (3.30e-3        210          103)      $ fe-54(n,p)mn-54
           (4.02e-6        211          102)      $ co-59(n,gamma)co-60
           (7.24e-3        212          103)      $ ni-58(n,p)co-58
           (2.10e-4        216          102)      $ mo-92(n,gamma)mo-93m
           (3.21e-4        217          102)      $ mo-98(n,gamma)mo-99
           (1.26e-4        218          102)      $ mo-100(n,gamma)mo-101
c     vanadium: 0.02 weight% added, note from Kalinin at NET (13.3.97)
           (1.86e-5        221          102)      $ v-51(n,gamma)v-52
c
  fc24  ----- activation of ss 1.4311, density = 7.876 g/cm3 -----
  f24:n    (103 108 113)  165    169      t       $ ports  torus  cryostat  total
  sd24        1.829e7   5.97e7 9.53e7  1.733e8    $ density * evaluated volumes
c         atoms/(b*cm)  mat.number  reaction path
  fm24:n   (7.42e-4        208          102)      $ cr-50(n,gamma)cr-51
           (1.72e-3        209          102)      $ mn-55(n,gamma)mn-56
           (3.57e-3        210          103)      $ fe-54(n,p)mn-54
           (4.02e-6        211          102)      $ co-59(n,gamma)co-60
           (5.57e-3        212          103)      $ ni-58(n,p)co-58
c     vanadium: 0.02 weight% added, note from Kalinin at NET (13.3.97)
           (1.86e-5        221          102)      $ v-51(n,gamma)v-52
c
  fc34  ----- activation of copper, density = 8.933 g/cm3 -----
  f34:n      164     184                          $ support_of_tiles  support_of_divertor
            (268 270)                             $ control_coils
             166     168                          $ heat_shields: torus  cryostat
             152     253                          $               mf_coils  af_coils
           (104 109 114)   t                      $               ports  total
  sd34     1.152e7  2.608e6                       $ density * evaluated volumes
           4.154e5
           1.733e6  3.913e6
           6.548e6  1.822e6
              2.894e6   3.146e7
c         atoms/(b*cm)  mat.number  reaction path
  fm34:n   (5.91e-2        213          102)      $ cu-63(n,gamma)cu-64
           (2.55e-2        214          102)      $ cu-65(n,gamma)cu-66
c
  fc44  ----- activation of superconductor, density = 4.064 g/cm3 -----
  f44:n      155     256       t                  $ mf_coil  auxiliary_coil
  sd44     5.405e7 5.974e6  6.003e7               $ density * evaluated volumes
c         atoms/(b*cm)  mat.number  reaction path
  fm44:n   (7.36e-5        202          102)      $ mg-26(n,gamma)mg-27
           (4.19e-2        203          102)      $ al-27(n,gamma)al-28
           (1.01e-5        204          102)      $ si-30(n,gamma)si-31
           (1.04e-4        207          102)      $ ti-50(n,gamma)ti-51
           (3.79e-6        208          102)      $ cr-50(n,gamma)cr-51
           (5.13e-6        210          103)      $ fe-54(n,p)mn-54
           (1.01e-2        213          102)      $ cu-63(n,gamma)cu-64
           (4.35e-3        214          102)      $ cu-65(n,gamma)cu-66
           (2.83e-3        215          102)      $ nb-93(n,gamma)nb94m
c
  fc54  ----- activation of solder, density = 10.50 g/cm3 -----
  f54:n      183                                  $ divertor
  sd54     5.135e4                                $ density * evaluated volumes
c         atoms/(b*cm)  mat.number  reaction path
  fm54:n   (3.42e-4        207          102)      $ ti-50(n,gamma)ti-51
           (1.39e-2        213          102)      $ cu-63(n,gamma)cu-64
           (6.00e-3        214          102)      $ cu-65(n,gamma)cu-66
           (2.30e-2        219          102)      $ ag-107(n,gamma)ag-108
           (2.10e-2        220          102)      $ ag-109(n,gamma)ag-110
c
  fc64  ----- activation of tzm, density = 10.20 g/cm3 -----
  f64:n      182                                  $ divertor
  sd64     2.50e6                                 $ density * evaluated volumes
c         atoms/(b*cm)  mat.number  reaction path
  fm64:n   (1.02e-2        216          102)      $ mo-92(n,gamma)mo-93m
           (1.56e-2        217          102)      $ mo-98(n,gamma)mo-99
           (6.09e-3        218          102)      $ mo-100(n,gamma)mo-101
c
  fc74  ----- activation of air -----
  f74:n      50   51   170     t                  $ from machine to wall
  sd74        1    1    1      1                  $ normalized volumes
c         atoms/(b*cm)  mat.number  reaction path
  fm74:n   (2.53e-7        205          102)      $ ar-40(n,gamma)ar-41
c
c #######################################################################################
c
c ----- ----- materials for activation calculations ----- -----
c
```

```
c      nuclide id   atom fraction                  isotop
c ---------------------------------------------------------------------------
 m202  12026.30y        1                        $ mg-26
 m203  13027.30y        1                        $ al-27
 m204  14030.30y        1                        $ si-30
 m205  18040.30y        1                        $ ar-40
 m207  22050.30y        1                        $ ti-50
 m208  24050.30y        1                        $ cr-50
 m209  25055.30y        1                        $ mn-55
 m210  26054.30y        1                        $ fe-54
 m211  27059.30y        1                        $ co-59
 m212  28058.30y        1                        $ ni-58
 m213  29063.30y        1                        $ cu-63
 m214  29065.30y        1                        $ cu-65
 m215  41093.30y        1                        $ nb-93
 m216  42092.30y        1                        $ mo-92
 m217  42098.30y        1                        $ mo-98
 m218  42100.30y        1                        $ mo-100
 m219  47107.30y        1                        $ ag-107
 m220  47109.30y        1                        $ ag-109
 m221  23051.30y        1                        $ v-51
c #####################################################################################
c
c ----- ----- general data cards ----- -----
  print 10                              $ source coefficients and distribution
        30                              $ tally description
        50                              $ cell volume and masses, surface areas
  mode    n                             $ transport calculations for n
  prdmp   j -120                        $ dump every 120 minutesc
  vol    no                             $ no volume calculation for activation
c  vol     1 135r                        $ all volumes set to 1
c  nps     1e5                           $ number of particle histories
  nps     1e4                           $ number of particle histories
c #####################################################################################
```

```
c #####################################################################################
c
c |_____data cards presently not in use_____|
c
c #####################################################################################
  fq0   e f                             $ fluxes: energies e are columns, cells f are rows
c
c ----- ----- current tallies ----- ----- current tallies ----- -----
  fc1   total neutron current at various surfaces
  c1    0 1                                  $ outward and inward directed current
  f1:n      511    512    513    514    520    521    522         $ torus and cryostat
         900 901 902 903  904 905 906  907 908 909  950 951 952   $ surrounding cylinders
  e1    1e-8 5e-8 2e-7 1e-6 5e-6 2e-5 1e-4
        5e-4 2e-3 1e-2 5e-2 2e-1 1 3     $ bounds of energy bins for neutron flux spectra
c
c ----- ----- surface flux tallies ----- ----- surface flux tallies ----- -----
  fc2   total surface flux at various surfaces (neutrons)
  f2:n      511    512    513    514    520    521    522         $ torus and cryostat
        (900 901 902 903)(904 905 906)(907 908 909)(950 951 952)  $ surrounding cylinders
  sd2    1.84e6 1.85e6 1.94e6 1.94e6 4.37e6 4.38e6 4.44e6         $ areas from test run
                j             j            j            j         $ calculated areas
  e2    1e-8 5e-8 2e-7 1e-6 5e-6 2e-5 1e-4
        5e-4 2e-3 1e-2 5e-2 2e-1 1 3     $ bounds of energy bins for neutron flux spectra
c
c ----- ----- volume flux tallies ----- ----- volume flux tallies ----- -----
  fc4   n-flux spectra in various cells (n/cm2)
  f4:n   161   163    164    165    166    168    169             $ toroidal components
         50 51 (50 51)
  sd4   5.43e6 1.83e6 1.29e6 7.58e6 1.94e5 4.38e5 1.21e7          $ volumes from test run
          j  j    j
  e4    1e-8 5e-8 2e-7 1e-6 5e-6 2e-5 1e-4
        5e-4 2e-3 1e-2 5e-2 2e-1 1 3     $ bounds of energy bins for neutron flux spectra
c
c  e4    1e-11 4.14e-7 3.93e-6 3.73e-5 3.54e-4 3.35e-3 3.18e-2 1.66e-1
c        3.02e-1 5.50e-1 6.72e-1 8.21e-1 1.00  1.225 1.653 2.231 2.725
c
c #####################################################################################
c
c #####################################################################################
c
c ----- ----- surface dose rates (n) ----- ----- surface dose rates (n)----- -----
```

```
  fc12  neutron induced dose rate at the inside and outside of concrete wall.
        flux across surfaces is multiplied by the energy dependent function:
        flux to dose rate conversion (mrem/hr)/(neutrons/cm^2*s) from ICRP-21.
        the tally multipier 87.6 (=8760 hours/year)/(100 rem/Sv)
        converts mrem/hr into mSv/year.
  fq12  e f                             $ table with row=surface and column=energy bin
  fm12  87.6
  f12:n 907 908 909 (907 908 909)       $ inside of concrete wall
        950 951 952 (950 951 952)       $ outside of concrete wall
  de12  2.50e-8 1.00e-7 1.00e-6 1.00e-5 1.00e-4 1.00e-3 1.00e-2
        1.00e-1 5.00e-1 1.00    2.00    5.00    10.0    20.0
  df12  3.85e-3 4.17e-3 4.55e-3 4.35e-3 4.17e-3 3.70e-3 3.57e-3
        2.08e-2 7.14e-2 1.18e-1 1.43e-1 1.47e-1 1.47e-1 1.54e-1
c       bounds of energy bins for neutrons
  e12   0.025e-6  0.5  2.5              $ thermal, epithermal, and fast neutrons
c
c ----- ----- surface dose rates (p) ----- ----- surface dose rates (p)----- -----
  fc22  photon induced dose rate at the inside and outside of concrete wall.
        flux across surfaces is multiplied by the energy dependent function:
        flux to dose rate conversion (mrem/hr)/(neutrons/cm^2*s) from ICRP-21.
        the tally multipier 87.6 (=8760 hours/year)/(100 rem/Sv)
        converts mrem/hr into mSv/year.
  fq22  e f                             $ table with row=surface and column=energy bin
  fm22  87.6
  f22:p 907 908 909 (907 908 909)       $ inside of concrete wall
        950 951 952 (950 951 952)       $ outside of concrete wall
  de22  0.01    0.015   0.02    0.03    0.04    0.05    0.06
        0.08    0.10    0.15    0.20    0.30    0.40    0.50
        0.60    0.80    1.0     1.5     2.0     3.0     4.0
        5.0     6.0     8.0     10.0
  df22 2.78e-3 1.11e-3 5.88e-4 2.56e-4 1.56e-4 1.20e-4 1.11e-4
       1.20e-4 1.47e-4 2.38e-4 3.45e-4 5.56e-4 7.69e-4 9.09e-4
       1.14e-3 1.47e-3 1.79e-3 2.44e-3 3.03e-3 4.00e-3 4.76e-3
       5.56e-3 6.25e-3 7.69e-3 9.09e-3
c
  void   11 12 13                        $ no material in the concrete wall
  void   50  51 103 104 108 109 113 114
        152 153 154 155 158 159
        161 163 164 165 166 168 169 170
        181 182 183 184 185
        253 254 255 256 258 259
        261 268 269 270 271
        358 359 361
        458 459 461
        558 559 561                      $ no material in the machine
c
c #####################################################################################
c ----- ----- data cards only for volume and area calculations (see p. 3-51) ----- -----
c
c ----- ----- surface source only for volume and area calculations (see p. 3-51) ----- -----
  sdef   sur=9999  erg=2.5           $ surface source of 2.5 mev neutrons
         nrm=-1    dir=d1            $ normal towards origin
         wgt=2.0428e7                $ weighted by pi*r2 (r=2550)
  sb1    -21 2                       $
c
c ----- ----- tallies only for volume and area calculations (see p. 3-51) ----- -----
  fc2   surface flux tallies to evaluate areas
  f2:n   511    512    513    514    520    521    522            $ torus and cryostat
  sd2   1.84e6 1.85e6 1.94e6 1.94e6 4.37e6 4.38e6 4.44e6          $ areas evaluated
c
  fc4   cell flux tallies to evaluate volumes
  f4:n   103    104    108    109    113    114                   $ ports type I and II
         152    153    154    155    253    254    255    256     $ mf- and af-coils
         158    258    358    458    558    (158 258 358 458 558) $ ring supp. for each section
         159    259    359    459    559    (159 259 359 459 559) $ x-elements for each section
         161    261    361    461    561    (161 261 361 461 561) $ plasma for each section
         163    164    165    166    168    169                   $ toroidal components
         181    182    183    184    185                          $ divertor
         268    269    270    271                                 $ control coils
  sd4   8.18e5 1.14e5 7.52e5 1.05e5 7.52e5 1.05e5                 $ volumes evaluated
        7.33e5 1.39e7 6.44e6 1.33e7 2.04e5 2.64e6 1.40e6 1.47e6
        1.14e6 1.14e6 1.14e6 1.14e6 1.14e6        5.70e6
        1.99e6 1.99e6 1.99e6 1.99e6 1.99e6        9.95e6
        5.43e6 5.43e6 5.43e6 5.43e6 5.43e6        2.72e7
        1.83e6 1.29e6 7.58e6 1.94e5 4.38e5 1.21e7
        4.27e5 2.45e5 4.89e3 2.92e5 3.25e5
        3.76e4 1.35e4 8.90e3 3.34e3
c
c ----- ----- end of data cards for volume and area calculations ----- -----
c #####################################################################################
```